First-Principles study of a few Pnictide Superconductors and Surface states of a Topological Insulator

A thesis submitted in partial fulfilment for the degree of

Master of Science (ENGINEERING)

by

WASIM RAJA MONDAL

Molecules to Materials Laboratory
Theoretical Science Unit
Jawaharlal Nehru Centre for Advanced Scientific Research
(A Deemed University)
Bangalore, India.

DECLARATION

I hereby declare that the matter embodied in the thesis entitled "**First-Principles Study of few Pnictide Superconductors and Surface states of a Topological Insulator**" is the result of investigations carried out by at the Theoretical Science Unit, Jawaharlal Nehru Centre for Advanced Scientific Research, Bangalore, India under the supervision of Prof. Swapan K. Pati and that it has not been submitted elsewhere for the award of any degree or diploma.

In keeping with the general practice in reporting scientific observations, due acknowledgement has been made whenever the work described is based on the findings of other investigators.

Wasim Raja Mondal

Wasim Raja Mondal

CERTIFICATE

I hereby certify that the matter embodied in this thesis entitled "**First-Principles Study of few Pnictide Superconductors and Surface states of a Topological Insulator**" has been carried out by Mr. Wasin Raja Mondal at the Theoretical Science Unit, Jawaharlal Nehru Centre for Advanced for Advanced Scientific Research, Bangalore, India under my supervision and that it has not been submitted elsewhere for any degree or diploma.

SPati

Prof. Swapan K. Pati

(Research Supervisor)

Acknowledgements

It is a great fortune to get an opportunity to acknowledge those people who motivate me from my childhood. Some of them stand by me; some of them assist me; whereas some of them bless me. I am grateful to all of them for their concern both in academic as well as personal life.

First of all, I would like to express my love and respect to my parents. I believe without them I would not be here.

I would like to thank my research supervisor, Prof. Swapan K. Pati for giving me the chance to work with him.

I would like to thank all my course instructors, Prof. Shobhana Narashimhan, Prof. Swapan K. Pati, Prof. Subir K. Das, Prof. Umesh V. Waghmare, Dr. N. S. Vidyhadhiraja and Prof. Aloknath Chakrobarty.

I would like to thank all my labmates, Prakash, Arun, Pralok, Dibya, Chaitanya, Bradraj, Arkamita, Swastika, Somananda, Ershaad, Alex, Wasim Aftab, Dr. Ganga, Dr.Siam, Dr. Mira, Dr. Elizabeth, and Dr. Mohakud. I would like to thank all my T.S.U friends.

I am really grateful to JNCASR for giving me wonderful environment for working. I want to thank all admin staff for their help.

Last but not the least, I would like to thank my teachers in school, college and university. I want to thank Dr. Dilip Roy, Dr. Krishnendu Mukherjee for motivating me.

Synopsis

This thesis presents studies on some pnictide superconductors and surface states of a topologic insulator. The present thesis is divided into four chapters.

Chapter 1 represents brief introduction of three new topics in condensed matter physics whi are developed last four years. These three topics are Iron-pnictide superconductors, Nicke pnictide superconductors and Topological insulators. In addition, there is complete descriptio of the method which is used for all the calculations.

Chapter 2 gives a detail study of electronic structure of platinum doped Iron-pnictid superconductor ($CaFe_{1-x}Pt_xAs_2$). The predicted electronic structure of the parent compound of th iron-pnictide superconductor is in good agreement with the experimental observation.

The first-principles based study on Nickel-pnictide superconductor ($BaNi_2As_2$) is described i chapter 3. The importance of structural phase transition for the increase in transition temperatur (T_C) of superconductors is shown in this chapter. The predicted structural phase transition is i good agreement with experimental observation. This study also predicts the reason behind the increase of T_C with this structural phase transition. This study shows the importance of phonon i this superconductor.

Studies on surface states properties of a topological insulator (Bi_2Se_3) are given in chapter 4. Experimentally observed surface states modification in the presence of water is tested in this study. This study explains some of the experimental observation.

List of Figures

List of Tables

Contents

Chapter 1

Introduction

Superconductivity is an exciting phenomenon of current flow with zero resistance. Besides the zero resistance, the superconducting material has a few exotic properties: (1) in the presence of the magnetic field from the interior of a superconductor magnetic lines of force are excluded (2) below a characteristic temperature (T_c) superconductivity can be destroyed by the application of external magnetic field which we call type-I superconductors and for type-II superconductors, superconductivity can be partially destroyed with the application of magnetic field H (Hc1<H<Hc2). Following the discovery of superconductivity by Onnes in 1911, a series of superconductors had been discovered and the transition temperature (T_C) kept on increasing. More than 2000 materials had been predicted to be superconducting by 1975 and T_C rose to 22.3 K with the appearance of Nb_3Ge superconductor [1] in 1973. Most successful BCS theory appeared in 1957. With the success of this theory, it was believed that higher transition temperature is not possible without new superconducting mechanism. Already in 1954, Fröhlich proposal [2] for the high temperature superconductivity in charge density wave system and in 1964 Little's excitonic superconductivity model [3] initialize the possibility of getting high temperature superconductors. In 1975, superconductivity was found in $BaPb_{1-x}Bi_xO_3$ with T_C= 13 K [4] which is regarded as the first oxide superconductor. A series of oxides had been found to be superconducting, for example, $PbMo_6S_8$ (T_C=16 K) [5], LaCuO3 [6], La_2CuO_4 (Tc=30 K) [7]. In February of 1987, Chu et al. predicted a new superconducting material, $YBa_2Cu_3O_7$ with

Tc=90 K [8]. This is most important breakthrough in the history of superconductivity. After this, Tc rose with great expectation in $Bi_1Sr_1Ca_1Cu_2O_x$ (Tc=105 K) [9], $TI_2CaBa_2Cu_2O_{8+\delta}$ (Tc=120 K) [10], $HgBa_2Ca_2Cu_3O_x$ (Tc=135 K but Tc=164 K under high pressure) [11].This observation called for a theory other than BCS theory. Alongside there was continuous effort to find non-copper based superconductors. The discovery of superconductivity in pnictides [12] is a great achievement in this field. Other than pnictides, superconductivity is found in many other non-copper based materials, for example, is alkali-ion doped C_{60} (Tc=33 K) [13], MgB_2 (Tc=39 K) [14], alkali-doped fullerene $RbCs_2C_{60}$ (Tc=33k under ambient pressure) [15]. But among all the non-copper based superconductors, pnictide is the most precious candidate due to two reasons. Firstly, the transition temperature (T_C) of Pnictides is the highest compared to other non-copper based superconductors. Secondly, the superconducting mechanism of pnictides is non-BCS type, which is quite similar to cuprate superconductors. On the other hand, superconductivity mechanism in other non-copper based materials except pnictides differs from cuprates. For example, superconductivity in alkali-ion doped C_{60} can be explained in terms of BCS theory. So pnictides can give us a new route towards high temperature superconductivity. Pnictide family consists of two types of superconductors. One is iron-pnictide superconductors and another is Nickel-pnictide superconductors.

In the last couple of years, the appearance of topological insulator is one of the most exciting phenomena in condensed-matter physics. It is a new quantum state of matter with special surface states property. The physics of surface state of topological insulators is quite interesting with valuable applications.

This chapter is divided into two sections: sections 1.1 and 1.2. Section 1.1 is divided into sections 1.1.1 and 1.1.2. In sections 1.1.1, we have given brief introduction of iron-pnictide

superconductors. We have introduced Nickel-pnictide superconductor in sections 1.1.2. In section 1.2, we have given brief description of topological insulators.

1.1.1 Iron-Pnictide superconductor

Iron-pnictide superconductors are chemical systems containing iron and pnictogen atoms with superconducting properties. Superconductivity in iron-based system [16, 17] with T_C=55 K motivates physicists to study its superconducting mechanism which is as rich as in cuprates.

There exist mainly four groups of iron-pnictide superconductors. First is the '1111' group with the composition MFeAsO, where M represents a lanthanide such as, La, Ce, Pr, Sm or Eu. The entire series of compounds under this group are particularly interesting due to their transition temperature which is as high as 55 K [16, 17]. These types of materials show superconductivity when doped with electrons. This is achieved by substituting oxygen with fluoride, or by simply reducing the oxygen content. The second group is the so-called '122', which has the composition MFe_2As_2, where M represents the alkali-earth elements. Superconductivity can be induced in these kinds of materials by doping with holes or by replacing alkaline-earth elements [18]. The third group is based on only Fe and one of the chalcogen elements. The most popular compound in this group is FeSe, where the transition temperature is found to be about 8 K, in the absence of externally applied pressure or doping. But this transition temperature can go up to 27 K [19] in the presence of doping or high pressure. The systems in this group are particularly interesting because of their simple structure. Fourth is the well known 21311 group, for example,

Sr_2ScO_3FeP system [20]. Transition temperature (T_C) of this system is 17K which can be increased 37K by substituting Sc by V and P by As, which can be seen in Sr_2VO_3FeAs [21].

It was believed that the iron-based superconductors are more complex than the cuprate superconductors. In cuprates, cupric ion (Cu^{2+}) has only one unfilled orbital. Hence, single narrow-band model containing both kinetic energy and onsite Coulomb interactions, for example, the Hubbard model, t-J model, in principle can describe all the major properties of the cuprates. On the other hand, in iron-pnictide, the Fe^{2+} has six electrons in five d orbitals. Moreover, electron filling in different orbitals depends on the competition between the Hund's coupling and the 'crystal field' splitting. This crystal field splitting is just lattice-potential-induced energy splitting between different d orbitals. Thus, a multi-band approach is more favorable for the study of iron-pnictides unlike cuprates.

A central issue in this field is whether the non-interacting band theory based on local density approximation (LDA) or generalized gradient approximation (GGA) can provide a suitable starting point for understanding the reason behind the superconductivity in iron-based superconductors. The undoped parent compounds in cuprates are Mott-insulators where carriers are localized because of the strong on-site Coulomb repulsions. This observation of parent compounds in cuprate makes the issue of electron-correlation in iron-pnictide more serious. But fortunately, the parent compounds in iron-based superconductors are quite different than that of cuprates. The parent compounds in iron-based superconductors are purely metallic, not Mott-insulating. This suggests that the electron correlation in iron-pnictide is not as strong as in cuprates. In cuprates, the bond-length between two copper atoms is quite large. This prevents the overlap between two Cu d orbitals. As a result, copper atoms are very much localized in cuprates. But in iron-pnictides, the bond-length between two iron-atoms is not as large as in

cuprates. The short bond distance between two Fe atoms helps in overlapping between Fe-3d orbitals of two neighboring Fe atoms. This might be one of the main reason why iron-pnictide is a good conductor at room temperature compared to cuprates[22]. Moreover, electron correlation in iron-pnictide is not local and estimated effective U is less than 0.5 eV [23]. This reduction of effective U is due to the hybridization between Fe-3d electrons with As 4p electrons. First principle based results are found to be in agreement with experimental observations to some extents [24]. Besides the low correlations, one of the major attractions of the iron-pnictide compound is the existence of magnetism. Magnetic ordering has been observed in iron-pnictides [25]. The nature of this magnetic order is long-range anti-ferromagnetic order with a simple stripe-type in the parent compound. There is competition between this magnetic ordering and superconductivity. Superconductivity wins due to suppression of the magnetic ordering by either electron or hole doping. This picture is very similar to cuprates.

The superconductivity in iron-pnictide is very much unconventional. The traditional BCS theory (26) which is based on electron-phonon coupling is not able to explain such high transition temperature in these systems. First-principle based computed electron-phonon coupling constant often fails to reproduce the experimental T_C value [27]. The reason behind this failure may be due to the spin fluctuations. It is believed that anti-ferromagnetic spin fluctuation plays the same role in these compounds as lattice vibrations in conventional superconductors.

The most key mystery of the unconventional superconductivity lies in its pairing mechanism. To correctly predict the pairing mechanism of Fe pnictide superconductors, it is necessary to predict the symmetry of their order parameter as the symmetry is directly related to the microscopic pairing mechanism in these systems. The symmetry of the order parameter in the conventional superconductors is isotropic s-wave. But the symmetry of the order parameter (Δ), in the

unconventional superconductors is different than the conventional superconductors. Many different types of possible symmetry of the order parameters have been proposed. These symmetries [28] are shown in figure 1:

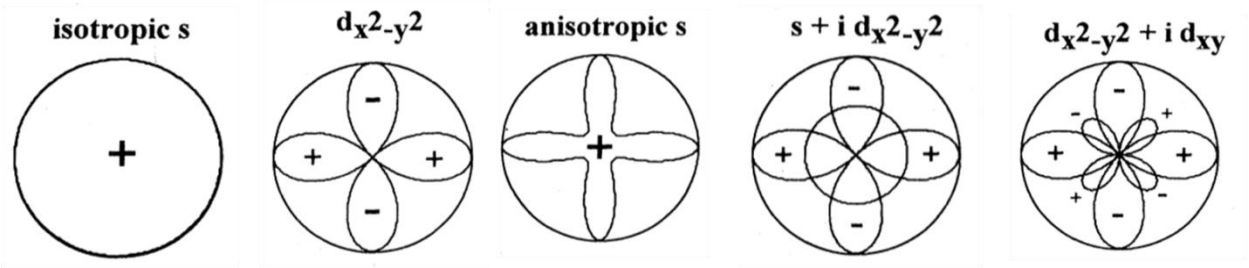

Figure 1. Different types of order parameter

In cuprates, the predicted order-parameter symmetry is d_{x2-y2} [29]. In the d-wave, the nature of the pairing is based on repulsion. But the Cooper pair wave function changes sign four times on circling the Fermi surface. This sign change may create attraction which helps in pairing. NMR relaxation rate and specific heat measurements indicate the existence of nodal lines with gapless quasi-particles at certain points on the Fermi surface [30]. This anticipation is supported by scanning tunneling microcopy (STM) and Andreev-reflection experiments on polycrystalline samples [31, 32]. STM data gives linear-in-energy dependence of the local density of states below T_C. Measurements of Andreev reflection shows a zero-bias peak which is due to an Andreev bound state at the Fermi surface. All these observations exclude the possibility of s-wave symmetry in high temperature pnictide superconductors. In this background, one ARPS measurement gave a new picture for pairing mechanism in pnictides which is completely different from cuprates. According to ARPS data on crystal samples of the 122 compounds [33], there is a fully gaped Fermi surface without any sign of nodal lines. This discrepancy from

cuprates gives a new challenge to the condensed-matter physicists to test the existing theory. Various efforts have been made to predict the pairing mechanism in iron-pnictides. It is believed that there are two kinds of symmetry existing in iron-pnictides. One is S_{+-} and the other is S_{++} symmetry. In S_{+-} symmetry, the pairing is due to spin fluctuation, whereas in S_{++} symmetry, the pairing is due to orbital fluctuation. Many studies have been devoted to correctly predict which symmetry of the order parameter exists in iron-pnictide and there are many controversial results. However, all the results about the pairing in iron-pnictide has one common similarity: lattice distortion with spin-density-wave (SDW) occurs at wave vectors (Π, 0) or (0, Π) in the parent non-superconducting compounds in the low temperature regime [34]. Application of increased doping or pressure [35] destroys the spin-density-wave (SDW) phase. In this context, 1111 and 122 families of the iron-pnictide systems show quite different behavior. Lattice distortion and spin-density-wave take place at two different transition temperatures [36] in 1111 compound, whereas, in the 122 compound, the lattice distortion and spin-density-wave occur at the same transition temperature with a finite jump in the structural lattice constants [37, 38]. Theoretical models [39, 40] have been proposed to find the reason behind this kind of behavior.

However, there are many mysteries, still alive in the iron-pnictide study. For example, magnetism in these systems is not fully understood. Total spin of one Fe ion is either 1 or 2 because Fe^{2+} has six electrons in the 3d orbitals. However, spin-density-magnetic moment in 1111 compound is found to be only 0.3 Bohr magnetons [41]. The consequence of metallic electron in iron-pnictide is an important issue.

1.1.2 Nickel-pnictide superconductors

The discovery of superconductivity in pnictide family is a major achievement after the prediction of superconductivity in copper-based materials. The most number of superconducting candidates of pnictide family are iron-based systems. Besides these iron-pnictide superconductors, the most promising candidate for superconductivity is Nickel-pnictide superconductors. Nickel-pnictide superconductors are chemical systems, consisting of nickel and pnictogen atoms. It has very low $T_{C,}$ but it shows quite interesting properties which has attracted much attention. Like iron-pnictides, Nickel-pnictides can also appear as oxy-nickel-pnictides and Non-oxy-nickel-pnictides. The representative candidate for oxy-nickel-pnictide superconductors is LaONiP [42] whereas the non-oxy-nickel-pnictide is $BaNi_2P_2$ [43]. Both of this systems (LaONiP and $BaNi_2P_2$) have same transition temperature (T_C=3 K). In spite of this low Tc, from structural point of view, nickel-pnictide superconductors are very similar to iron-pnictides. It has also layered structure of nickel atoms with pnictogen atoms stacked above and below these planes. Like iron-pnictides, superconductivity can be induced with the application of external pressure. The Tc value in nickel-pnictide superconductors is very much sensitive to structural distortion. Electronic correlation is very low in these superconductors. All these properties of Nickel-pnictides can help us to know what parameters are responsible for high T_C which can be tuned to look for new high temperature superconductors.

1.1.3 Topological Insulator

Band Theory of solid based on translational invariance in crystal lattices and Bloch theorem helps us to know the band structures of solid and why a solid is a metal, an insulator or semiconductor. In recent years, a new class of materials has attracted much attention in condensed-matter physics due to its peculiar property, that its bulk is insulating while its surface or edge states are metallic. The material with this new kind of feature is called Topological insulator. The metallic behavior in surface states of topological insulator is quite robust against impurities or interaction and protected by the presence of time reversal symmetry. These kinds of materials are characterized by an inverted energy gap which is caused by spin-orbit coupling (SOC). The surface states of topological insulators differ from ordinary metals in the sense that these surface states show linear dispersion, forming a Dirac cone at or near the Fermi level. Another interesting feature of the topological insulator surface states is that it carries only a single electron per momentum with a spin that changes its direction with the change in momentum.

The origin of the discovery of topological insulator lies in the discovery of Hall family of systems. One parameter scaling theory [44] in 1979 predicted that the localization of all electrons in two or lower dimensions occur even with a very weak disorder. This theory gives a new shape to the research on lower dimensional systems with disorders or interactions. Almost at the same

time, the experimental discovery of integer quantum Hall Effect (IQHE) [45] gave a new excitement to this field. Two years later, Tsui et al. predicted fractional Hall Effect (FQHE) [46]. From theoretical point of view, edge state electrons form discrete landau levels in the presence of strong magnetic field in IQHE. Electrons near the boundary jumps along the boundary to form a conducting channel [47, 48], while the group velocity of electrons in the bulk is zero. Thus in IQHE, all bulk electrons are insulating due to localization while the edge electrons show metallic behavior because these edge electrons form several conducting channels based on the electronic density, which is considered as robust against the impurities. With this feature, IQHE gives the indication of a new state of quantum matter which is now known as topological insulators. In the case of FQHE, the electrons are incompressible due to electron-electron interaction and form metallic edge states which are quite stable [49, 50].

Unlike the other fields of condensed matter physics, the Dirac equation is popular in the study of topological insulators. It appears in this field due to two reasons. Firstly, because the topological insulators have strong spin-orbit coupling.This is considered as a direct consequence of Dirac equations. It essentially couples the spin, momentum and the Coulomb interactions or external electric fields together. That is why; we see band structures of some materials are topologically non-trivial. Another reason is that the effective Hamiltonians to the QSHE and 3D topological insulators posses same mathematical structure of the Dirac equation. One of the remarkable properties of the Dirac equation is that this equation is invariant with respect to time-reversal symmetry which plays the key role in the topological insulators. From the solution of modified Dirac equation, it is found that the edge states and surface states exist at the interface of systems with positive and negative masses. But there is positive-negative mass symmetry in the Dirac equation. Thus it is difficult to distinguish between trivial and non-trivial surface states. Hence,

Dirac equation alone can not describe the topological insulators. To explore the complete picture of topological insulators, one has to consider the modified Dirac equation.

A topological insulator is characterized by four Z2 [51] topological invariants ($\nu_1, \nu_2, \nu_3, \nu_4$). It can be termed as strong topological insulators or weak topological insulators [52]. One of the features of topological insulator is the existence of surface states on the Fermi surface. A topological insulator with odd number of surface states is considered as strong or non-trivial topological insulator, and one with even number of surface states is termed as a weak or trivial topological insulator. So far, all the topological insulators are related with band inversion. In fact, there are five groups of materials in three dimensional topological insulator families. First group is trivial topological insulator group. The representatives of this family are PbTe and SnTe, where SnTe is the first inverted band material discovered around fifty years ago. The example of second family member is bismuth antimony alloy ($Bi_{1-x}Sb_x$) [53, 54] which is the first three dimensional strong topological insulator. This alloy is particularly interesting because of its rich property of thermoelectric power. The third member is 3D topological insulator with single Dirac cone. Example of these types of topological insulators are Bi_2Se_3 [55] and Bi_2Te_3 [56]. Both of these topological insulators have simple and robust surface states consisting of a single Dirac cone [57]. Fourth type is strained 3D HgTe type-topological insulator. Other materials are expected to be topological insulator, like, Half-Heusler compounds (LaPtBi).

The applications of topological insulators, in spintronics or magnetoelectric devices, make them much more valuable than the ordinary semiconductors. Topological insulators in combination with superconductors can give us a new root for topological quantum bits. Besides that, it has

huge application in quantum computation. Many exciting phenomena like Majorana fermion can be realized in terms of these topological insulators.

Density Functional Theory

1.2.1 Introduction

The main aim of most of the studies in solid state physics is the solution of the time-independent Schrödinger equation which is given by

$$\hat{H}\Psi_i(\vec{x}_1, \vec{x}_2, \ldots, \vec{x}_N, \vec{R}_1, \vec{R}_2, \vec{R}_M) = E_i \Psi_i(\vec{x}_1, \vec{x}_2, \ldots, \vec{x}_N, \vec{R}_1, \vec{R}_2, \ldots, \vec{R}_M) \qquad (1.1)$$

where $\hat{H}$ is the Hamiltonian for a system consisting of M nuclei and N electrons. In expanded form, it can be written as

$$\hat{H} = -\frac{1}{2}\sum_{i=1}^{N}\nabla_i^2 - \frac{1}{2}\sum_{A=1}^{M}\frac{1}{M_A}\nabla_A^2 - \sum_{i=1}^{N}\sum_{A=1}^{M}\frac{Z_A}{r_{iA}} + \sum_{i=1}^{N}\sum_{j>1}^{N}\frac{1}{r_{ij}} + \sum_{A=1}^{M}\sum_{B>A}^{M}\frac{Z_A Z_B}{R_{AB}} \quad (1.2)$$

Throughout this section, all quantities are reported in atomic unit. Here A and B sums are over the M Nuclei while i and j describe the N electrons in the system. M_A is the mass and Z_A is the charge of the A th nuclei. r_{iA} is the distance between ith electron and Ath nuclei while r_{ij} is the distance between ith and jth electron and R_{AB} is the distance between nuclei A and B.

The first two terms in Eq. 1.2 represent the kinetic energy of the electrons and nuclei respectively. The other three terms describe the attractive electrostatic interactions between the

nuclei and the electrons and repulsive potential due to the electron-electron and nucleus-nucleus interactions respectively.

Complete solution of equation (1.1) is difficult in principle because the associated wave function in this equation is a function of 3N variables, where N is the total number of electrons and nucleus in the system. To solve equation (1.1), the first approximation that one adopts is the Born-Oppenheimer approximation. According to this approximation, due to the heavy masses of nuclei compared to electrons, the nuclei move much slower than the electrons and we can think of the electrons as moving in the field of fixed nuclei. Thus the nuclear kinetic energy becomes zero and their potential energy is almost constant. Under this approximation, the Hamiltonian in equation (1.2) reduces to the following equation.

$$\hat{\mathrm{H}}_{elec} = -\frac{1}{2}\sum_{i=1}^{N}\nabla_i^2 - \sum_{i=1}^{N}\sum_{A=1}^{M}\frac{Z_A}{r_{iA}} + \sum_{i=1}^{N}\sum_{j>1}^{N}\frac{1}{r_{ij}} = \hat{\mathrm{T}} + \hat{\mathrm{V}}_{\mathrm{Ne}} + \hat{\mathrm{V}}_{\mathrm{ee}} \quad (1.3)$$

Now the solution of the schrödinger equation (1.1) with $\hat{\mathrm{H}}_{elec}$ as given in equation (1.3) is the electronic wave function Ψ_{elec} and E_{elec} , the electronic energy. Thus the total energy $\mathrm{E}_{\mathrm{tot}}$ is the sum of E_{elec} and the constant nuclear repulsion term $\mathrm{E}_{\mathrm{nuc}}$

.

$$\hat{\mathrm{H}}_{elec}\Psi_{elec} = \mathrm{E}_{elec}\Psi_{elec} \quad (1.4)$$

$$\mathrm{E}_{\mathrm{tot}} = \mathrm{E}_{elec} + \mathrm{E}_{nuc} \quad (1.5)$$

Where

$$\mathrm{E}_{nuc} = \sum_{A=1}^{M}\sum_{B>A}^{M}\frac{Z_A Z_B}{R_{AB}} \quad (1.6)$$

Using the simplified Hamiltonian in equation (1.3), the eigenvalue equation (1.4) can be solved for fixed nuclear configurations to obtain the electronic energy eigenvalue. But still the full quantum mechanical solution is not possible because it has 3N degrees of freedom, where N is the number of electrons present in the system. To solve the many-body equation as given in equation (1.4), we have to consider further approximation like Hartree-Fock theory, Density Functional Theory etc.

1.2.3 Hohenberg-Kohn Theorems

In 1964, Hohenberg and Kohn proposed two theorems [44] that connect the exact solution of the many body Hamiltonian.

Theorem I For any system of interacting particles in an external potential V_{ext} (r), the external potential is determined uniquely except for a constant by the ground state particle density, ρ (r).

Theorem II A universal functional of energy E[n], in terms of density, ρ(r), can be defined for any external potential, V_{ext} (r) ,the exact ground state energy of system is global minimum value of this functional and the density ρ(r) which minimizes the functional is the exact ground state density.

$$E_{HK}[\rho] = \int \rho(\vec{r}) V_{ext}(\vec{r}) d\vec{r} + F_{HK}[\rho] \qquad (1.11)$$

$$F_{Hk}[\rho] = T[\rho] + E_{ee} \qquad (1.12)$$

Thus these two theorems first time gave the existence of the functional $F_{HK}[\rho]$, however could not predict any practical way to determine $F_{Hk}[\rho]$ or the ground state density. After one year of these two theorems, in 1965 Kohn and Sham proposed a way to solve this issue.

1.2.4 Kohn-Sham Ansatz

The idea of Kohn-Sham was to replace the exact Hamiltonian of an interacting many-body system by a fictitious non-interacting single particle Hamiltonians, which can be solved easily.

$$E[\rho] = Ts[\rho] + \frac{1}{2}\iint \frac{\rho(r_1)\rho(r_2)}{r_{12}} d\vec{r}_1 d\vec{r}_2 + E_{xc}[\rho] + \int V_{Ne}\,\rho(\vec{r})d\vec{r} \quad (1.13)$$

where the first term on the right hand side represents the kinetic energy of electrons, the second term is the electrostatic interaction energy between electrons; the third term is exchange correlation interaction between electrons, and the fourth term is the interaction energy of electrons with external potential.

Khon-Sham equation for the non-interacting system is given by

$$[\nabla^2 + V_{KS}]\Psi_i(r) = \varepsilon_i \Psi_i(r)$$

Where

$$V_{KS}(\vec{r}_1) = \int \frac{\rho(\vec{r}_2)}{r_{12}} d\vec{r}_2 + V_{ext}(\vec{r}) + V_{xc}(\vec{r}_1) \qquad (1.19)$$

First term in the above equation (1.19) is the Hartree potential, second term is external potential and third term is the exchange correlation potential and is given by

$$Vxc = \frac{\delta E_{xc}[\rho(r)]}{\delta\rho(r)}$$

This potential is not known and it has to be approximated.

1.2.5 Approximation for the exchang-correlation functional

Two well known approximations for the exchange-correlation functional are local density approximation (LDA) and generalized gradient approximation (GGA).

The local density approximation (LDA) is simplest among all the approximations for the exchange-correlation functional. LDA is based on the idea of uniform electron gas. In uniform electron gas, electrons move on a positive background charge distribution such that total charge is zero. In LDA, the exchange-correlation functional can be written as

$$E_{xc}^{LDA}[\rho] = \int \rho(\vec{r})\varepsilon_{xc}(\rho(\vec{r}))d\vec{r} \qquad (1.20)$$

where $\varepsilon_{xc}(\rho(\vec{r}))$ represents the exchange-correlation energy per particle of homogenous electron gas of density $\rho(r)$. This quantity can be divided into exchange and correlation contribution,

$$\varepsilon_{xc}(\rho(\vec{r})) = \varepsilon_x(\rho(\vec{r})) + \varepsilon_c(\rho(\vec{r})) \qquad (1.21)$$

The exchange part (ε_x) describes the exchange energy of an electron in a homogenous electron gas. The analytical form was first derived by Bloch and Dirac in the late 1920's which is given as

$$\varepsilon_x = -\frac{3}{4}\left(\frac{3\rho(\vec{r})}{\pi}\right)^{1/3} \qquad (1.22)$$

However, there is no such explicit form exists for the correlation part (ε_C). But the approximate forms of ε_{xc} is given by Ceperley and Alder using quantum Monte Carlo [45]. Later Perdew and Zunger parameterized it using simple analytical expression [46].

The exchange-correlation energy for homogenous charge density and non-homogenous charge density differ significantly. This difference can be predicted by considering the gradient of the charge density. The central idea of GGA is not to use only charge density but the gradient of the charge density in order to account for the non-homogeneity of the true electron density. Thus within GGA, the exchange-correlation energy can be written as

$$E_{xc}^{GGA} = \int \rho(\vec{r})\varepsilon_{xc}(\rho(\vec{r}), \vec{\nabla}\rho(\vec{r}))d\vec{r} \qquad (1.23)$$

For GGA, more advanced approximations for exchange-correlation functional have been developed by Perdew, Burke, Ernzerhof (PBE) [47], Perdew and Wang (pw91) [48] and Becke(B88) [49].

1.2.6 Basis set

The most common method for the solution of single-particle Kohn-Sham equations for the extended system like crystalline solid is to expand the single-particle Eigen states of the Kohn-Sham equations into a set of basis functions. Many different kinds of basis sets can be used. These are plane-wave basis set, atomic-orbital basis sets, mixed (plane-wave + atomic orbital) basis sets. Among all the basis sets, plane wave basis has many advantageous for extended

systems for example pulay forces are absent and Hellmann-Feynman theorem is applicable for calculating forces.

1.2.7 Pseudopotentials

For practical application, the core electrons behavior can be ignored for most of the properties of solids because the core electrons do not take part in chemical bonding. This approximation has the following advantage:

(1) Within this approximation, fewer electrons need to be treated and calculations have to be done for less eigenstates of the Kohn-Sham equations.

(2) Because of this, the total energy scale would be greatly reduced in the calculations.

The Coulomb potential between the valance electrons and the nucleus in the core region is divergent. Due to this divergence of the Coulomb potential, there is large oscillation in the wavefunction of the valance electrons in the core region. It demands large basis set and calculations become expensive. To overcome this difficulty, the original potential can be substituted by a artificially constructed smooth and weaker potential. This kind of potential is called pseudopotential [50, 51, and 52]. It acts on a set of pseudo wavefunction rather than the original valance electron wave function.

For generation of pseudopotential, one has to first define one central quantity, cut off radius (r_c) which differentiate between the core and the valance region. The region within the r_c is considered as core region and region outside the r_c is treated as valance region. The value of r_c

has to be chosen carefully so that the last node of all electron wavefunction must fall within r_c . Pseudopotential and all electron wavefunction must be identical outside the core region. The pseudopotential wavefunction should be continuously differentiable at least twice at the cutoff radius, r_c.

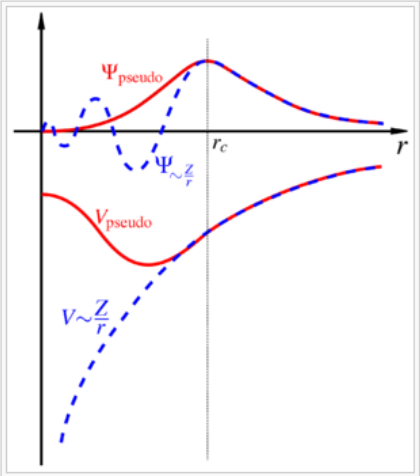

There are many kinds of pseudopotentials. These are norm-conserving pseudopotential and ultrasoft pseudopotential[53]. For norm-conserving pseudopotential, total charge within the cutoff radius for pseudo wavefunctions and all electron wavefunctions are equal. For this type of pseudopotential, pseudowavefunction also satisfy the orthogonality conditions

$$\left\langle \Phi_i \mid \Phi_j \right\rangle = \delta_{ij}$$

In ultrasoft pseudopotential, the constraints of norm conservations and orthogonality have been removed. This ultrasoft pseudopotential is much softer than the norm conserving

pseudopotential. But in ultrasoft pseudopotential, extra care should be taken for the charge density because it has to be augmented in the core region for recovering the full electronic

charge. The use of ultrasoft pseudopotential needs for treatment of KS equations in terms of generalized eigenvalue formalism.

Software used

All the calculations in this thesis were carried out using quantum espresso package. Xmgrace package was used for plotting. All the graphical analyses and visualizations were carried out by Gauss View [60] and Xcrysden [61] packages. Gimp was used for beautification of the picture.

Outline of the thesis

There are four chapters in this thesis. In chapter 2, we present a complete electronic structure of Pt-doped iron-pnictide superconductor, $CaFe_{1-x}Pt_xAs_2$. Our study gives an overview of complete electronic behavior of the parent compound of this iron-pnictide superconductor. Chapter 3 is devoted to the study of structural phase transition in $BaNi_2As_2$ superconductor. Our first-principle based results reproduce and explain the experimental fact for the structural phase transition in this nickel-pnictide superconductor. Finally, in chapter4, we give an introductory study on the surface states of topological insulator, Bi_2Se_3 .

Reference

(1) Matthias, B. T.; Geballe, T. H.; Willens, R. H.; Corenzwit, E.; Hull, G. W. Phys. Rev.139, 1501-1503, (1965)

(2) H. Fröhlich: Proc. Roy. Soc. A223, 296 (1954).

(3) W.A. Little: Phys. Rev. A134, 1416 (1964).

(4) A.W. Slight, J.L. Gillson and F.E. Bierstedt: Solid State Commun. 17, 27 (1975).

(5) M. Marezio, P.D. Dernier, J.P. Remeika, E. Corenzwit, B.T. Matthias. Material. Research. Bulletin, 8, 657-658, (1973)

(6) J.G. Bednorz and K.A. Müller: Z. Phys. B64, 189 (1986)

(7) H. Takagi, S. Uchida, K. Kitazawa and S. Tanaka: Jpn. J. Appl. Phys. 26, L 123 (1987)

(8) M.K. Wu, J.R.Ashburn, C.J.Torng, P.H. Hor, R.L. Meng, L.Gao, Z.J.Haung,Y.Q.Wang and C.W.Chu. Phys.Rev.Lett.58, 908-910 (1987)

(9) Maeda, Hiroshi; Tanaka, Yoshiaki; Fukutomi, Masao; Asano, Toshihisa; Togano, Kazumasa; Kumakura, Hiroaki; Uehara, Mitsuru; Ikeda, Syozo; Ogawa, Keiichi; Horiuchi, Shigeo; Matsui, Yoshio. Physica C, 153,602-607 (1988)

(10) L. Gao, Z. J. Huang, R. L. Meng, P. H. Hor, J. Bechtold, Y. Y. Sun, C. W. Chu, Z. Z. Sheng and A. M. Hermann. Nature 332, 623-624 (1988)

(11) C. W. Chu, L. Gao, F. Chen, Z. J. Huang, R. L. Meng and Y. Y. Xue. Nature 365, 323-325, (1993)

(12) Yoichi Kamihara, Takumi Watanabe, Masahiro Hirano and Hideo Hosono. J. Am. Chem. Soc., 2008, 130 (11), pp 3296–3297

(12) Gao, L.; Xue, Y. Y.; Chen, F.; Xiong, Q.; Meng, R. L.; Ramirez, D.; Chu, C. W.; Eggert, J. H.; Mao, H. K. Physical. Rev. B 50, 4260-4263 (1994)

(13) R.C. Haddon, A.S. Hebard, et al. : Nature 350, 320 (1991).

(14) Jun Nagamatsu, Norimasa Nakagawa, Takahiro Muranaka, Yuji Zenitani and Jun Akimitsu, Nature 410, 63 (2001).

(15) V Buntar and H W Weber. Supercond. Sci. Technol. 9 (1996) 599–615

(16)Zhi-An Ren, Guang-Can che, Xiao-Li Dong, Jie Yang, Wei Lu, Wei Yi, Xiao-Li shen, Zheng-Cai Li, Li-Lung Sun, Fang-Zhou and Zhong-Xian Zhao. *Europhys.Lett. 83, 17002 (2008).*

(17)X.H.Chen, T.Wu, G.Wu, R.H.Liu, H.Chen and D.F.Fang. *Nature 453,761-762 (2008)*

(18) Sasmal, K. et al. *Phys. Rev. Lett. 101, 107007 (2008)*

(19) Mizuguchi, Y., Tomioka, F., Tsuda, S., Yamaguchi, T. and Takano,Y. *Appl.Phys.Lett 93, 152505 (2008)*

(7) T.M.Mcqueen. et al. *Nature Materials 8, 630-633 (2009)*

(20) Ogino H, Matsumura Y, Katsura Y, et al. *Supercond Sci Technol, 22, 075008 (2009)*

(21) Zhu X, Han F, Mu G. et al. *Phys. Rev B, 79, 220512(R) (2009)*

(22) Johrendt D and Pottgen R. *Angew. Chem. Int. Edn, 47, 4782 (2008)*

(23) E. Aktürk1 and S. Ciraci. *Phys. Rev B, 79,184523 (2009)*

(24) Lu, D. H. et al. *Nature, 81, 455 (2008).*

(25) De la Cruz, C. et al. *Nature, 899–902, 453 (2008).*

(26) Bardeen J, Cooper L N and Schrieffer J R. *Phys. Rev, 108, 1175-204 (1957)*

(27)T.Yildrim. Phys.Rev.Lett. 102, 037003 (2009)

(28) J. Van. Hariingen. *Rev. Mod. Phys, 67, 515-535 (2005)*

(29) Nakai, Y., Ishida, K., Kamihara, Y., Hirano, M. & Hosono, H. J.Phys. Soc. Jpn, 77, 7 (2008)

(30) Wang, Y. et al. Supercond. Sci. Technol, 22, 015018 (2008)

(31) Millo, O. et al. Phys. Rev. B 78, 092505 (2008).

(32) Ding, H. et al. Europhys. Lett. 83, 47001 (2008).

(33) De la Cruz, C. et al. Nature 453, 899–902 (2008).

(34) Zhao, J. et al. Nature Materials,7, 953-959 (2008)

(35) McGuire, M. A. et al. Phys. Rev. B 78, 094517 (2008)

(36) Krellner, C. et al. Phys. Rev. B 78, 100504(R) (2008).

(37) Zhao, J. et al. Phys. Rev. B 78, 140504 (2008)

(38) Fang, C., Yao, H., Tsai, W.-F., Hu, J. P. & Kivelson, S. A. Phys. Rev B, 77, 224509 (2008)

(39) Xu, C., Müller, M. & Sachdev, S. Phys. Rev. B 78, 020501(R) (2008).

(40) Wei-Bing Zhang, Xiao-Bing Xiao, Wei-Yang Yu, Na Wang, and Bi-Yu Tang, Phys.Rev.B,77, 214513 (2008)

(41) Takashi Mine, Hiroshi Yanagi, Toshio Kamiya, Yoichi Kamihara 2, Masahiro Hirano and Hideo Hosono, Solid State Comm.147, 111 (2008)

(42) E. Abrahams, P.W. Andersons, D.C. Licciardello and T.v. Ramakrishanan. Phys. Rev. Lett, 42, 673 (1979).

(43) K.V. Klitzing and G. Dorda, M. Pepper. Phys.Rev.Lett, 45, 494 (1980)

(44)D.C.Tushi, H.L.Stromer and A.C. Gossard. Phys.Rev.Lett, 48, 1559 (1982)

(45) B.I.Halperin. Phys.Rev B, 25, 2185 (1982)

(46) R.B.Laughlin. Phys.RevB,23,5632 (1981)

(47) J. K. Jain. Phys.Rev.Lett, 63,199-202 (1989)

(48) R.B.Laughlin. Phys.Rev.Lett, 50, 1395 (1983)

(49) C.L.Kane and E.J.Mele.Phys.Rev.Lett,95,146802 (2005)

(50) Liang Fu and C.K. Kane. Phys.Rev B,76,045302 (2007).

(51) Shuichi Murakami .New J. Phys. 9, 356, (2007)

(52)D. Hsieh1, D. Qian1, L. Wray1, Y. Xia1, Y. S. Hor2, R. J. Cava2 & M. Z. Hasan,Nature,452,970-974 (2008)

(53) Y.xia, D.Qian, D.Heish,L.Wray, A.Pal, H.Lin,A.Bansil,D.Grauer,Y.S.Hor,R.J. Cava and M.Z.Hasan.Nature,Physics, 5, 398-402 (2009)

(54) Y.L.Chen,J.G.Analytis, J.H.Chue, Z.K.Liu,S.K.Mo, X.L.Qi,H.J.Zhang,D.H.Lu,X.Dai,Z. Fang,S.C.Zhang,I.R.Fisher,Z.Hussian,Z.X.Shen. Science 325, 178 (2009)

(43) Haijun Zhang1, Chao-Xing Liu2, Xiao-Liang Qi3, Xi Dai1, Zhong Fang1 & Shou-Cheng Zhang, Nature Physics 5,438-442 (2009)

(44)P. Hehenberg and W. Khon, Phys. Rev.136, B864 (1964)

(45)D.M. Ceperley, and B.J. Alder. Phys.Rev.Lett, 45, 566, (1980)

(46)J.P.Perdew and A.Zunger. Phys.Rev.B 23, 5048 (1981)

(47)J.P.Perdew, K. Burke and M. Ernzerhof. Phys.Rev. Lett. 80, 891 (1998)

(48)Y.Wang and J.P.Perdew, Phys.Rev. B 43, 8911 (1991)

(49)A.D.Becke, Phys.Rev.A 38, 3098 (1998)

(50)J.C. Phillips. Phys.Rev,112,685 (1958)

(51)J.C.Phillips and L.Kleinman, Phys.Rev, 116,287 (1959)

(52)M.L.Cohen and V. Heine. Solid State Physics 24, 37 (1970)

(53)D.Vanderbilt.Phys.Rev. B, 7892 (1990)

(54)H.J.Monkhorst and J.D. Pack, Phys.Rev.B 13,5188 (1976)

(55)C.L. Fu and K.M. Ho,Phys.Rev.B 28,5480 (1983)

(56)M.Methfessel and A.T. Paxton, Phys.Rev.B,40,3616 (1989)

(57)N.Marzari, D.vanderbilt, A.D. Vita, and M.C. Payne, Phys.Rev.Lett.82, 3296 (1999)

(58)O.H.Nielsen and R.M. Martin, Phys. Rev.Lett, 50, 697 (1983)

(59) O.H.Nielsen and R.M. Martin, Phys. Rev. B, 32, 3780 (1985)

(60) Gaussview3.0, Gaussian, Inc

(61) A.kokalj.comp.Mater.sci, 28, 155-168 (2003)

Chapter 2

Electronic structure of Pt-doped superconductor $CaFe_{1-x}Pt_xAs_2$

2.1 Introduction

Since the discovery of copper oxide (YBaCuO) high temperature superconductors (HTS) with transition temperature (TC) 93 K in 1987 [2], there have been innumerable research in finding cuprates with higher and higher T_C. Up to year 2009, the highest-temperature superconductor found is cuprate-perovskite ($HgBa_2Ca_{m-1}Cu_mO_{2m+2+\Delta}$) [62] with T_C 164 K under quasi hydrostatic pressure. At the same time, there have been efforts to synthesize similar type of superconductors other than cuprates. Some examples are MgB_2 (T_C 39 K) [63], Cs_3C_{60} (T_C 38 K) [64]. In the meantime, prediction of superconductivity in iron-pnictide ($La[O_{1-x}F_x]FeAs$, T_C=26K) has attracted much attention [65]. In particular, the transition temperature (T_C) in $SmO_{1-x}F_xFeAs$ is found to be 55 K [3]. Thus iron-pnictide superconductors become one of the centers of interest in the field of superconductors. Such high transition temperature like that of cuprates is very unconventional and becomes more challenging as BCS theory cannot explain the microscopic mechanism behind high-temperature superconductivity. Again, these iron-pnictides are becoming very significant because its similarities with cuprates which can provide us appropriate starting point to predict superconducting mechanism in cuprates.

Recently, an iron-pnictide superconductor, CaFe1-xPtxAs2, has been synthesized by Kawamata et. al. [66]. Two types of structures have been reported for this compound, $SrZnBi_2$ (type-A) and $HfCuSi_2$ (type-B). The space group of type-A is I4/mmm and that of type-B is p4/nmm. Type-A structure has two $Fe_{1-x}Pt_xAs$ layers whereas type-B has only one layer. Actually, there is difference in the stacking of layers along the c-axis. (Fig. 2.1 (a), 2.2 (b)). It has been found that there is small difference in the transition temperature (T_c) of these two structures, where type-A has T_c =29.3 K and for type-B it is T_c=30.1 K. The novelty of this compound is that, it acts as a HTS in the presence of large fraction of dopants like platinum and it does not has s_{+-} ordered parameter symmetry. But, surprisingly $CaFe_2As_2$ is not superconducting in the presence of Pt dopants [67]. That is why; $CaPt_xFe_{1-x}As_2$ is interesting and demands theoretical understanding for its observed behavior. In this work, we study both type-A and type-B structures. We have computed the electronic structure and its properties using density functional theory. In this paper, we mainly concentrate on the following questions in order to understand the physics of this system. (1) What kind of magnetic ordering is present in the parent compound of this superconductor? (2) Besides the dominant contribution of Fe '*3d*' orbitals, what is the role of doped Pt atom in the electronic structure of the system? (3) What is the role of topology of Fermi surface in the pairing mechanism? (4) What is the nature of the bonding between Fe and As? (5) What is the symmetry of the superconducting order parameter?

2.2 Computational Detail

Estimated effective U for the case of iron-pnictides is assumed to be less than 0.5. This value is reduced by hybridization of localized Fe '*3d*' electrons with As '*4p*' electrons [68], and hence we can apply band theory for iron-pnictides. Our results are based on first-principles pseudo potential-based density functional theory (DFT) as implemented in the PWSCF package [69]. We use ultra-soft pseudo potentials [70] to describe the the interaction between ion core and outer electrons and plane-wave basis set with kinetic energy cut-off 300 Ry for charge density and 30 Ry for wave functions. We consider generalized gradient approximation using Perdew-Burkew-Enzerhoff parameterized for the exchange correlation function. For spin ordered phases, we perform spin-polarized calculations with different initial spin configurations. For type-A, we consider unit cell but for type-B we consider 1×1×2 super-cell for comparison with type-A. We take 9×9×3 Monkhorst-pack mesh [71] for the integration over the Brillouin zone for both types of structures. Optimization is done by energy minimization in the Broyden-Fletcher-Goldfarb shanno(BFGS) [72]-based method. For the metallic behavior of the system, we use Methfessel-paxton scheme [73] with a smearing width of 0.003 Ryd for the occupation numbers. Structural Optimization is carried out with total energy difference between last two consecutive steps less than 10^{-8} Ryd, the maximum force on each atom less than 0.002 Ry/ au.

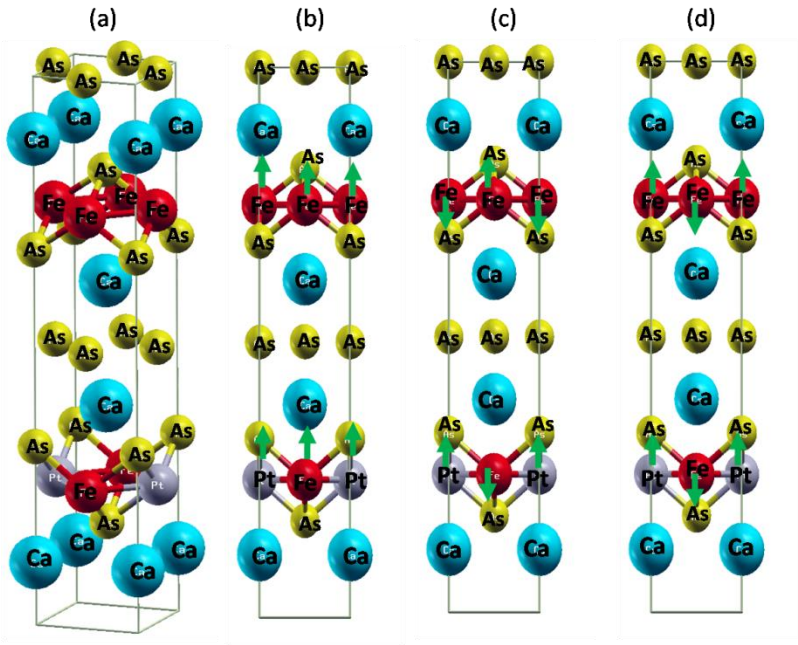

Figure 2.2: (a) crystal structure of type-A configuration. Ths schematic diagrams of different spin ordering on the Fe atoms in the unit cell, (b)Ferromagnetic ordering, (c)antiferromagnetic (AFM1) ordering, (d)antiferromagnetic strip(AFM2) ordering.

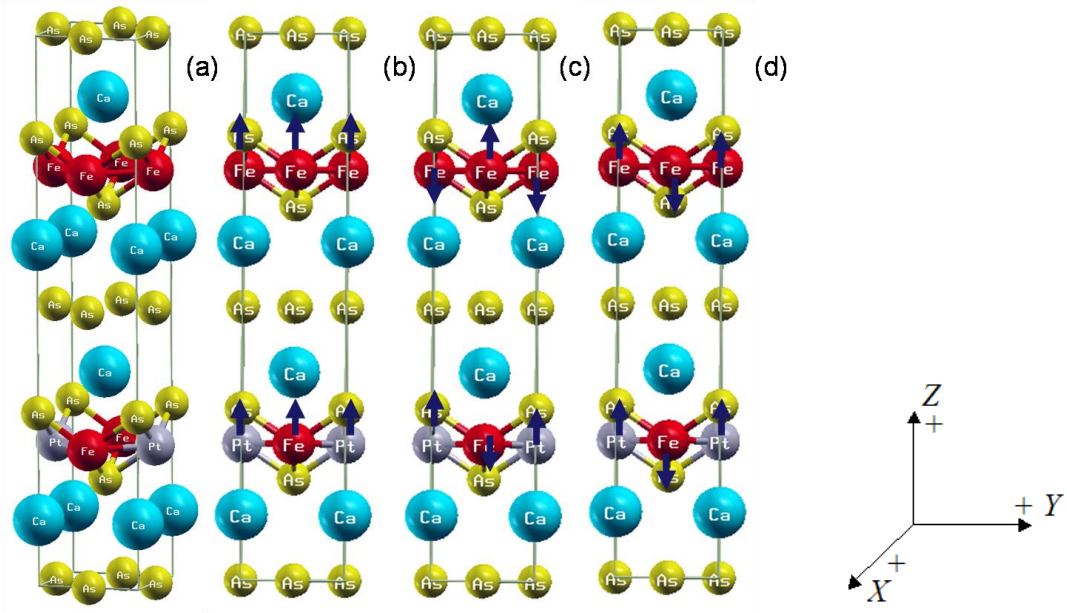

Figure 2.3: (a)Crystal structure of type-B configuration. (b)FM ordering (c) AFM1 ordering (d) AFM2 ordering

Table 1.Energy value of different spin-configuration and absolute magnetic moment(|M|in for eachFe) of the system (type-A).Total energies (eV) are given of all the spin configurations with respect to the total energy of non-mgnetic (NM)state.

States	Energy(eV)	Absolute Magnetic Moment $\|M\|(\mu_B)$
AFM2	-0.213	1.947
AFM1	-0.210	1.945
FM	-0.044	0.940
NM	0.000	0.000

Table 2.Optimized lattice parameters of the Pt-doped crystal, internal structure parameters (ZCaI and ZCaII), and bond-length between Fe-Fe of the system. Here ZCaI and ZCaII are the height of Ca atom from above and below the Fe-layer respectively.

States	Lattice parameter (Å)		$Z_{ca\text{-}I}$	$Z_{Ca\text{-}II}$	Bond(Å) (Fe-Fe)
	a	c			
AFM2	3.971	20.338	0.1365	0.1355	2.80
AFM1	3.974	20.295	0.1364	0.1355	2.81
FM	3.951	20.281	0.1383	0.1306	2.79
NM	3.935	20.169	0.1376	0.1315	2.78
EXPT.[66]	3.920	20.716	0.1305	0.1305	2.77

Table 3. Energy value of different spin-configuration and absolute magnetic moment(|M| in μ_B for each Fe) of the system (type-B). Total energies are given for all the spin configurations with respect to the total energy of the non-magnetic(NM) state.

states	Energy (eV)	Absoulete magnetic moment (|M|(μ_B)
AFM2	-0.216	1.94
AFM1	-0.149	1.16
FM	-0.04	2.19
NM	0.00	0.00

Table 4.Optimized lattice parameters of the Pt-doped crystal (type-B), internal structure parameters (ZCaI and ZCaII) and bond-length between Fe-Fe of the system. Here ZCaI and ZCaII are the height of Ca atom from above and below the Fe-layer respectively.

states	Lattice parameter a (Å)	Lattice parameter c(Å)	Z_{CaI}	Z_{CaII}	Bond(Å) (Fe-Fe)
AFM2	3.965	20.385	**0.135**	0.134	2.80
AFM1	3.945	20.328	0.135	0.134	2.79
FM	3.92	20.81	0.135	0.134	2.77
NM	3.933	20.208	0.137	0.130	2.78
EXPT.[66]	3.902	21.024	0.130	0.130	2.77

2.3 Results and Discussion

The structure is optimized with respect to both atomic positions and experimental lattice constants. To investigate the role of magnetic ordering on the electronic properties, we consider non-magnetic and different magnetically order phases depending on the spins on Fe atoms. In the ferromagnetic phase (FM), all spins on Fe atoms are in same direction in both y and z direction whereas in the G-type anti-ferromagnetic (AFM1) phase, these spin-ordering is anti-ferromagnetic in y-direction but ferromagnetic in z-direction. In the case of anti-ferromagnetic stripe (AFM2) phase, spin-ordering is anti-ferromagnetic in both y and z-direction. All these spin configurations are given in Fig. 2.1 and Fig. 2.2.

Our estimated energies of the different spin configurations for type-A are given in Table1. We find that AFM2 phase is energetically more stable with respect to all the other spin-configurations. The anti-ferromagnetic stripe (AFM2) phase is energetically more stable than the nonmagnetic phase (NM) by -0.213 eV/unit cell but the energy difference between anti-ferromagnetic striped (AFM2) and G-type anti-ferromagnetic (AFM1) phase is 3 meV/unit cells. Hence, G-type anti-ferromagnetic (AFM1) phase can be one of the meta-stable states of the system. But the large difference in energy of AFM2 phase and NM phase clearly indicates the importance of magnetic ordering in the structural stability of the system. Our calculated lattice parameters are presented in Table 2. In the case of AFM2 phase, calculated value of lattice parameter ‘a’ is 1.28% larger than the experimental value and lattice parameter ‘c’ is 1.8% smaller than the

experimental value. From Table 2, it is clear that there is significant difference between the calculated and experimental Z_{CaI} and Z_{caII} which is the height of pnictogen atom (Ca) from iron-arsenide plane. In the case of the Type-B system, we again find the AFM2 phase energetically more stable than any other spin configuration of this system as shown in Table 3. The calculated lattice parameter ‘a’ is 1.5% larger and lattice parameter ‘c’ is 3.1% smaller than the experimental value [66]. Like type-A system there is also a significant difference in the separation of Ca atoms from Fe-plane.

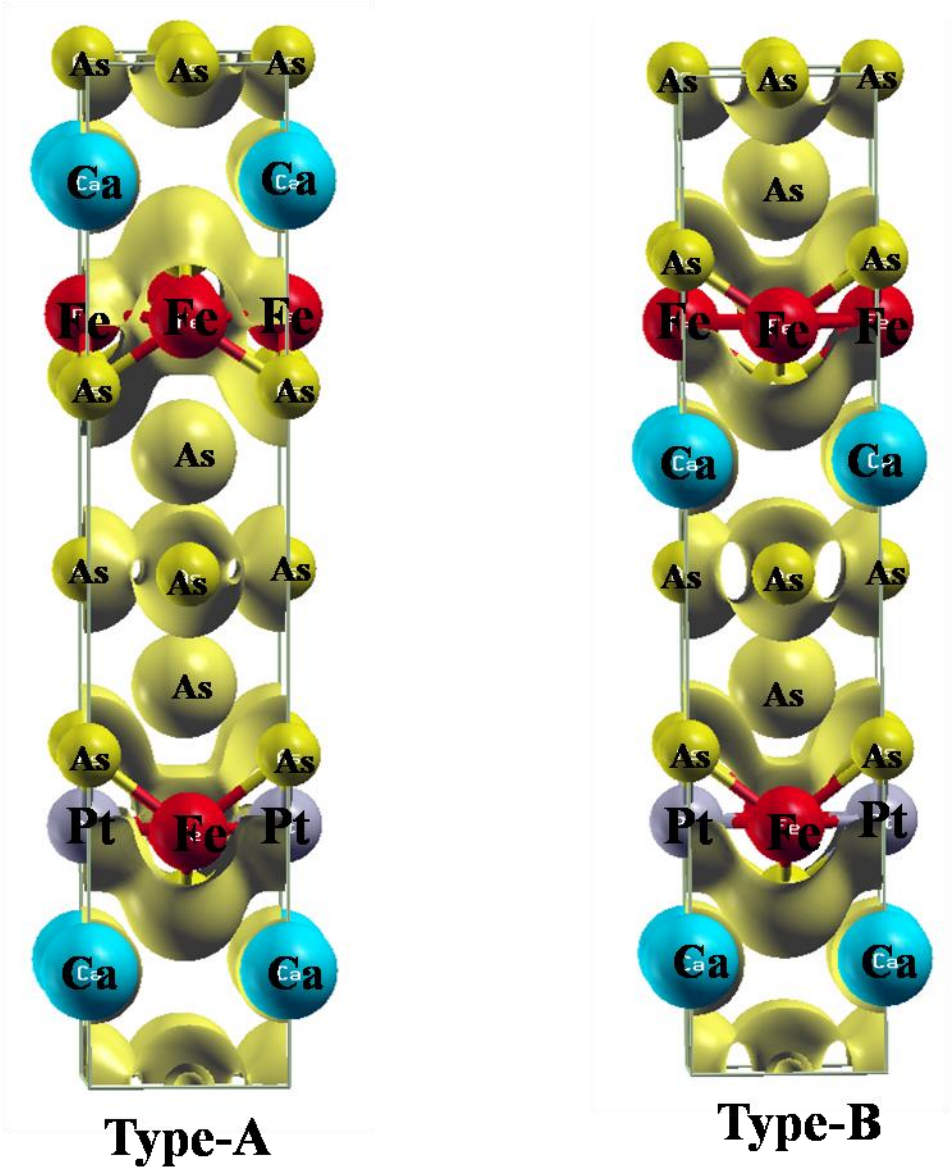

Figure 2.4: Charge density plot for type-A and type-B structure.

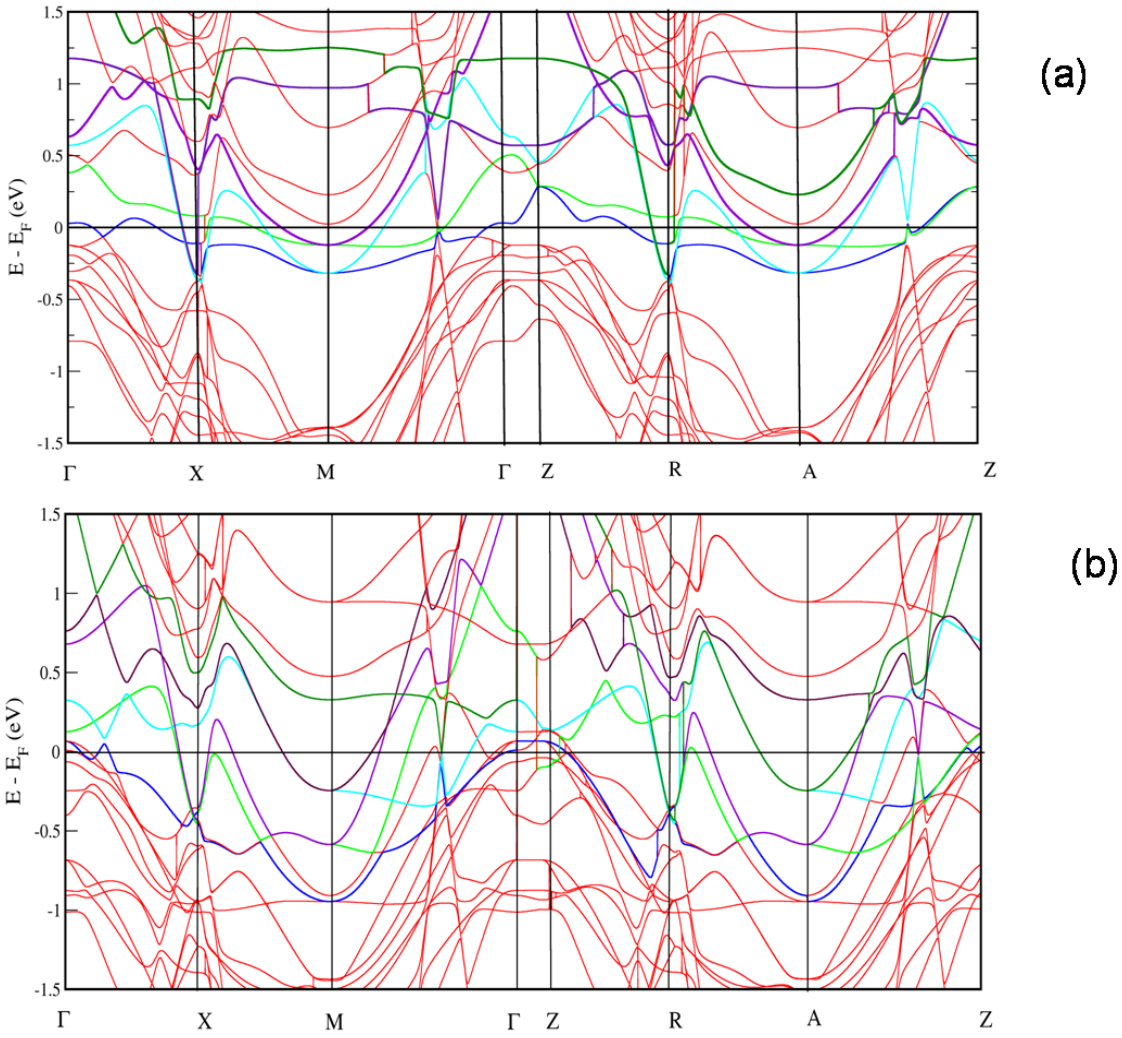

Figure 2.5: Electronic band structure of type-A: (a) NM phase, (b) AFM2 phase.

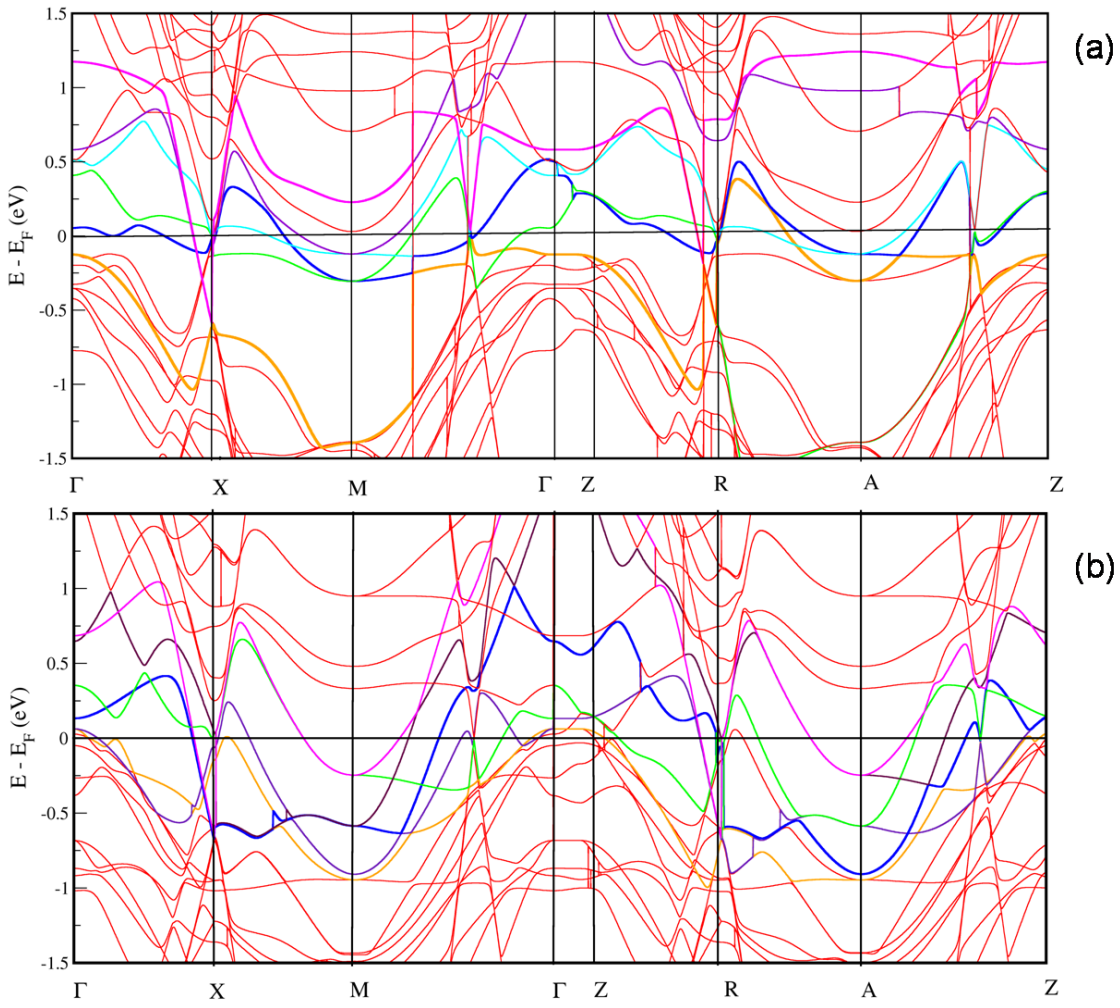

Figure 2.6: Electronic band structure of the type-B: (a) NM phase, (b) AFM2 phase.

Hence in both the structures, we find that the lattice parameters show anisotropic deformation of the crystal structure due to presence of magnetic ordering. For both Type-A and Type-B, in the optimized structures with different magnetic ordering, there exists a variation of pnictogen height where a small variation of pnictogen height gives a drastic change in the electronic structure as reported in Refs. [74]. This suggests that, AFM2 stripe phase is an important state of the parent compound of this high temperature superconductor. From data of Table 1 and Table 3, it is interesting to note that magnetic moment in AFM2 stripe phase is maximum compared to all other spin configuration in both type-A and type-B structure. In addition, lattice distortion in AFM2 stripe phase is also maximum along z direction. That means, lattice parameter along z direction increases with the increase in magnetic moment value. To understand this behavior we have plotted charge distribution for both the configuration in Fig. 2.3. There is a significant overlap between the electron cloud of Fe '3d' and As '4p' orbital (see Fig. 2.3). Besides this, there is also overlap between As 4p electrons between each other. This tells us the hybridization character between Fe 3d with As 4p electrons. Change in lattice parameter 'c' can be understood under the following way as described by Yildirim [16]:

Pnictogen atom such as As situated symmetrically top and below the iron-plane. There is tendency of overlap of As ions above the Fe-plane with the As ions below the same iron-plane. There are also interactions between Fe and As. This Fe-As interaction increases due to increase in Fe-moment. This increase in Fe-As interaction prevents to overlap of As ions above the iron-plane with As ions below the iron-plane. That is why; we observe the increase of lattice parameter c with the increase in Fe-moment. But it is interesting to note that, our calculated value of c parameter is not that much deviated

from experimental value as predicted by Yildrim in $CaFe_2As_2$ system. In our system, we have substituted Fe by Pt partially. This substitution decreases the magnetic moment. Hence, we have not observed that much strong increase in lattice parameter c value as found in $CaFe_2As_2$

Our calculated band structures for $CaFe_{1-x}Pt_xAs_2$ system with both I4/mmm symmetry and p4/nmm symmetry at the equilibrium lattice parameters along various high-symmetry points are given in Fig. 2.4 and Fig. 2.5. To understand the role of magnetism, we have investigated the band structures for both NM and AFM2 states of the systems. The overall band structures of both type-A and type-B configurations show the same features. We observe that overall band structures for both the phases (NM and AFM2) are same except that there is splitting of the degenerate energy states of NM phase in AFM2 phase. This is due to the broken symmetry of the AFM2 striped phase because in this phase spin ordering is antiferromagnetic along y direction but ferromagnetic long z direction. In the band diagrams, bands are highly dispersive and we do not observe any flat-bands near the Fermi level in both (AFM 2 and NM) configurations. Since electrons near the Fermi-level play a crucial role in the formation of the superconducting state, we analyze the electronic structure near the Fermi level. Bands near the Fermi level (in the range from -1.5 eV to +1.5 eV) comes mainly from Fe 3d states with small contribution of Pt '1d' and As '*2p*' states. We consider this system metallic rather than semi metallic in the sense that there are six bands crossing the Fermi level along the Γ-Z line. These bands with energies of 0.03eV, 0.39eV, 0.57eV, 0.65eV and 2.03eV at the Γ- point as shown in Fig. 2.4 and Fig. 2.5. Most of them cross the Fermi level in the directions Γ-X, Γ-M, R-A, Z-A in the Brillion zone and create the complex shape of the Fermi surface (see Fig. 2.7).

The bands that intersect the Fermi-level along the X-Γ direction, form electron-like sheet of the Fermi surface and bands cross the Fermi-level in the direction of M-R create hole-like sheet of the Fermi surface. Hence in the Fermi surface, we observe small hole-pocket at the Z-point and electron-pocket at the M point (see Fig. 2.6 and Fig. 2.7).

To explore the possible order-parameter for this system, we examine the band structure and Fermi-surface more closely. Generally, d_{x2-y2} order parameter will be most effective when the majority of states are found near (π,o,k_z) and equivalent points, while the s_{+-} order parameter will be considered when the majority of states are found near the (0,0,k_z) and (π,π,k_z) points [75]. In most of the iron-pnictide study, we observe the combination of hole pocket at the Γ point, and an electron pocket at the X point of the unfolded Brillion Zone. This is not the case in CaFe1-xPtxAs_2. Our calculation shows that there are significantly no states available for superconductivity near Γ-point and no large cylindrical Fermi surface at (π, π, k_z). This predicted result is similar with very recent report on Ce- and Pu- based superconductor (115 family) [75]. We find small hole pocket centered at the Z point and electron pocket centered at M point (see Fig 2.6 and Fig 2.8). Another interesting feature of this Fermi surface is that it has low dispersion along k_z direction. Hence our finding excludes the possibility of s_{+-} symmetry of the superconducting order parameter. This observation is consistent with the experimental prediction of the symmetry of the superconducting order parameter of this system [66].

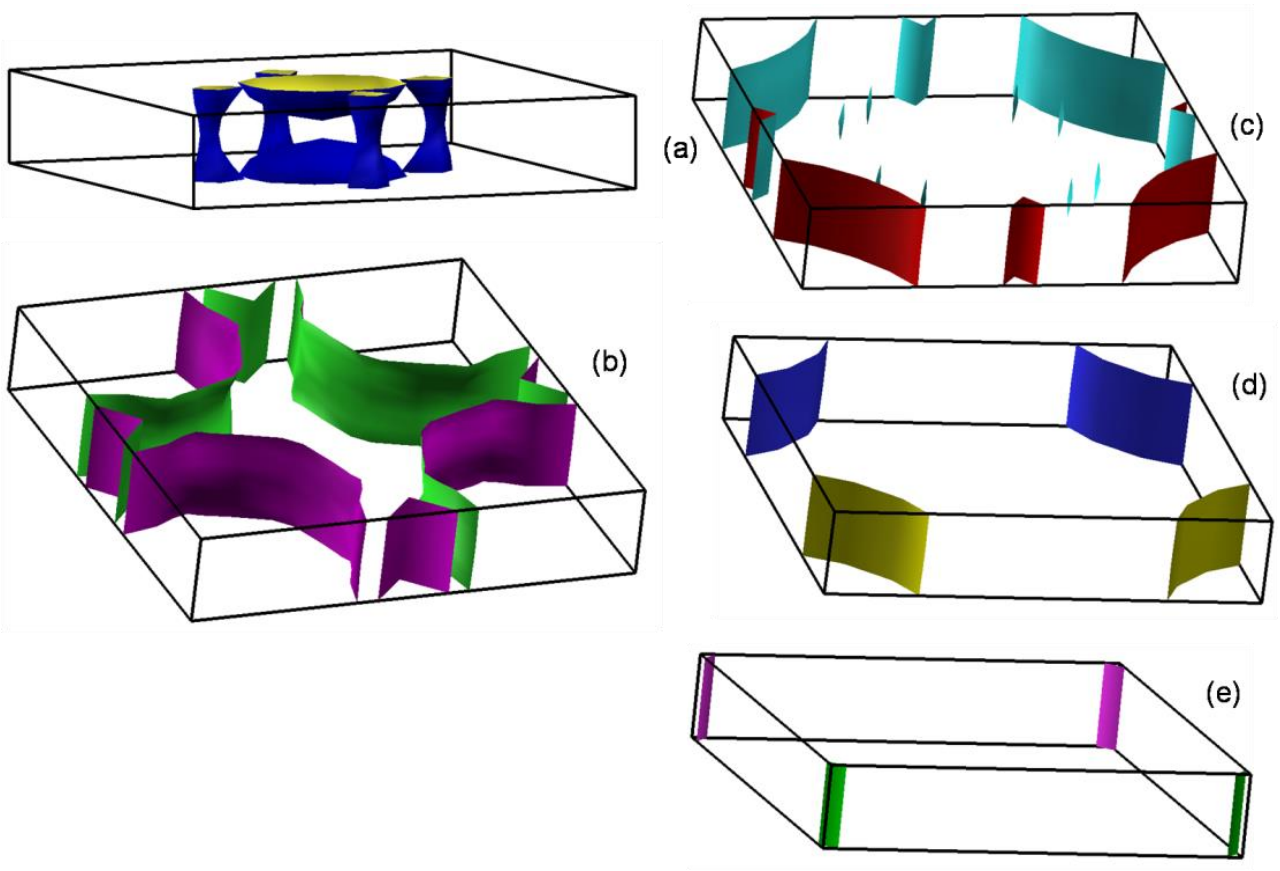

Figure 2.7: Separate sheets of the Fermi surface for type-A configuration. Four of them (b,c,d,e) are electroniclike, and sheet (a) is holelike

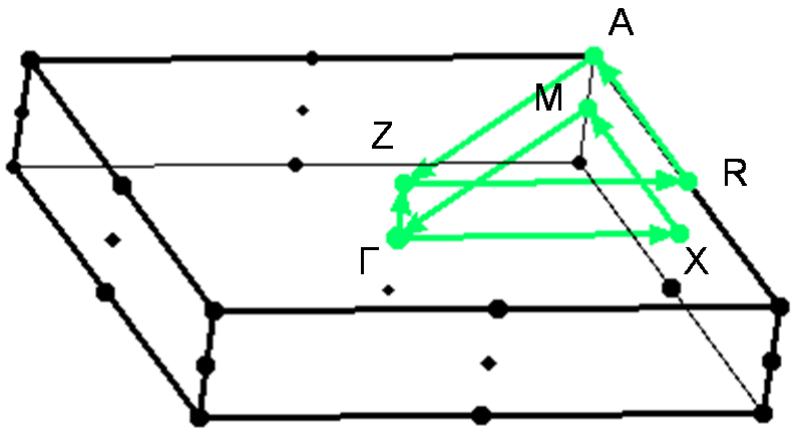

Figure 2.8: Diagram of path taken in brillouin zone along different symmetry point.

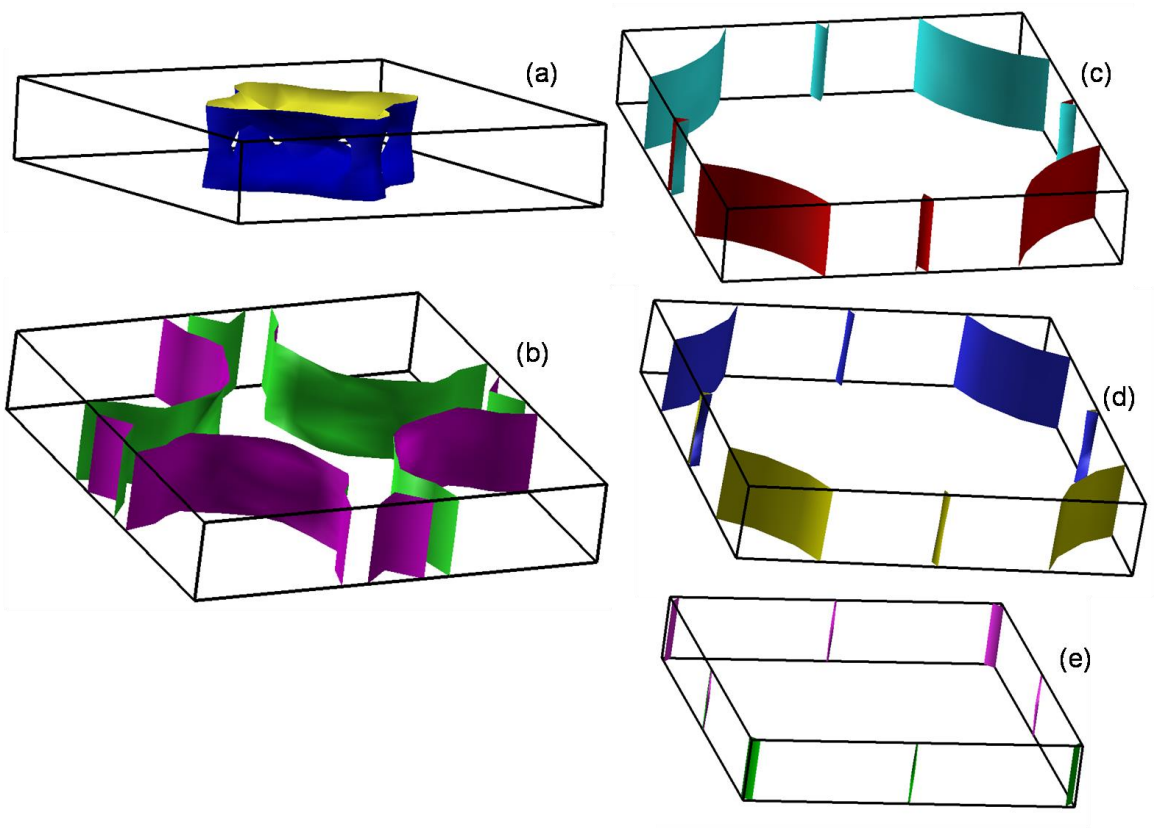

Figure 2.9: seperate sheets of the Fermi surface for type-B configuration. Four of them (b,c,d,e) are electron-like and sheet (a) is hole like

From the density of state plots of both the states (AFM2 and NM) in figure 9 and figure 10, we find that there is finite density of states in the Fermi level which shows the metallic character and agrees with experimental findings. The difference in the electronic structure of AFM2 and NM phase will be clear if we compare the density of states of these two phases. At the Fermi energy for the NM phase the density of state $N(E_F)$ =11.21 and for AFM phase $N(E_F)$=6.37 (see Fig. 2.9 and Fig. 2.10). From the orbital density of states which is shown in Fig. 2.11, we find that contribution of Fe '*3d*' orbital to the density of states $N(E_F)$ is dominant at the Fermi level . Clearly, this is due to the effect of direct intra-layer Fe-Fe interactions. This feature is consistent with the other layer-type tetragonal Fe-based superconductors.[33-34] The bandwidth of the Fe band around the Fermi level is about 4eV (-2 eV to +2 eV). In this energy ranges, besides the dominant contribution of Fe '*3d*' orbital, there is a small contribution of As '2p' and Pt '1d' orbitals too. We find that Fe 3d states overlap with As 2p states at -2 eV. This p-d hybridization makes Fe-As bonding strongly covalent. There is also a significant contribution from Pt '1d' orbital because of high concentration Pt doping. However, there is negligible contribution of Ca atoms to the total density of states at the Fermi-level. So Fe-layers containing Fe '*3d*' orbitals play the key role in the electronic structure of the system. In Fig. 2.12, we have plotted also the contribution of different Fe '*3d*' orbital for both type-A and type-B systems. Both the systems show a common feature. For both the systems, the spin-up and spin-down components of Fe atoms are partially filled. This kind of occupation of Fe '*3d*' state reveals the origin of the calculated local magnetic moment 1.94 μ_B of Fe atom in the AFM2 stripe phase for both Type-A and Type-B structure.

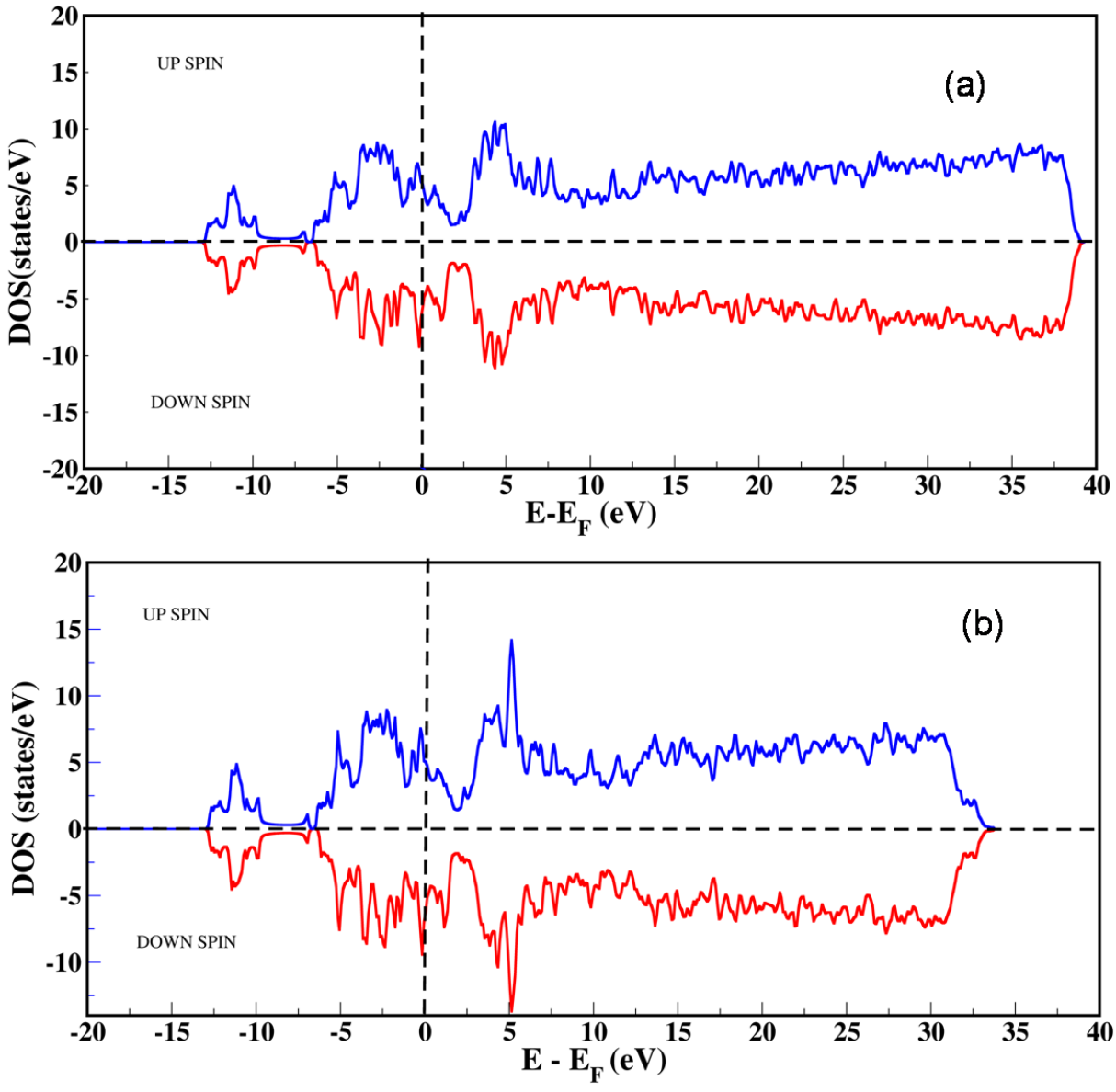

Figure 2.10: Density of states plot for AFM2 stripe-phase: (a) type-A (b) type-B

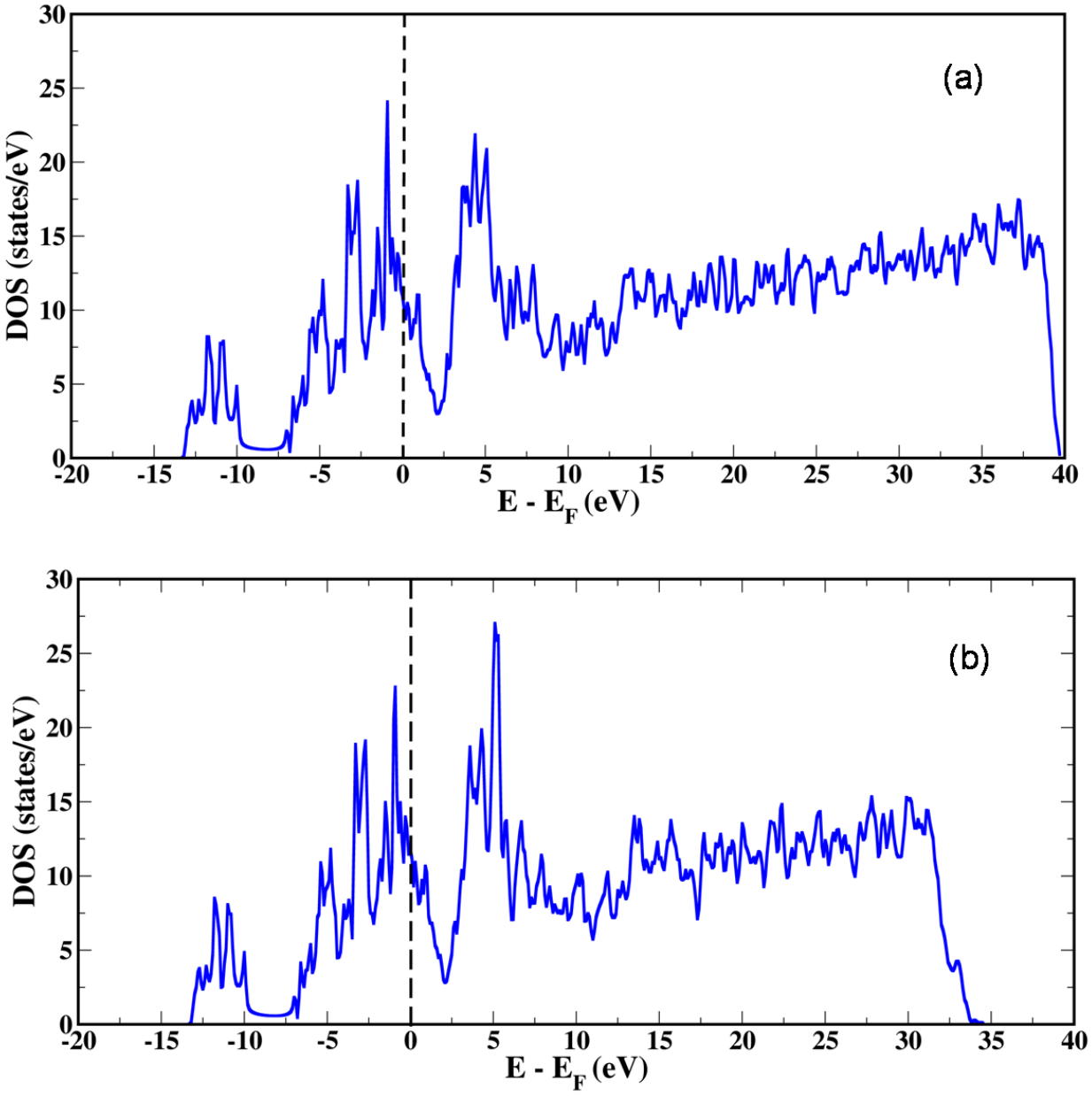

Figure 2.11: Density of states for non-magnetic (NM) phase: (a) type-A (b) type-B

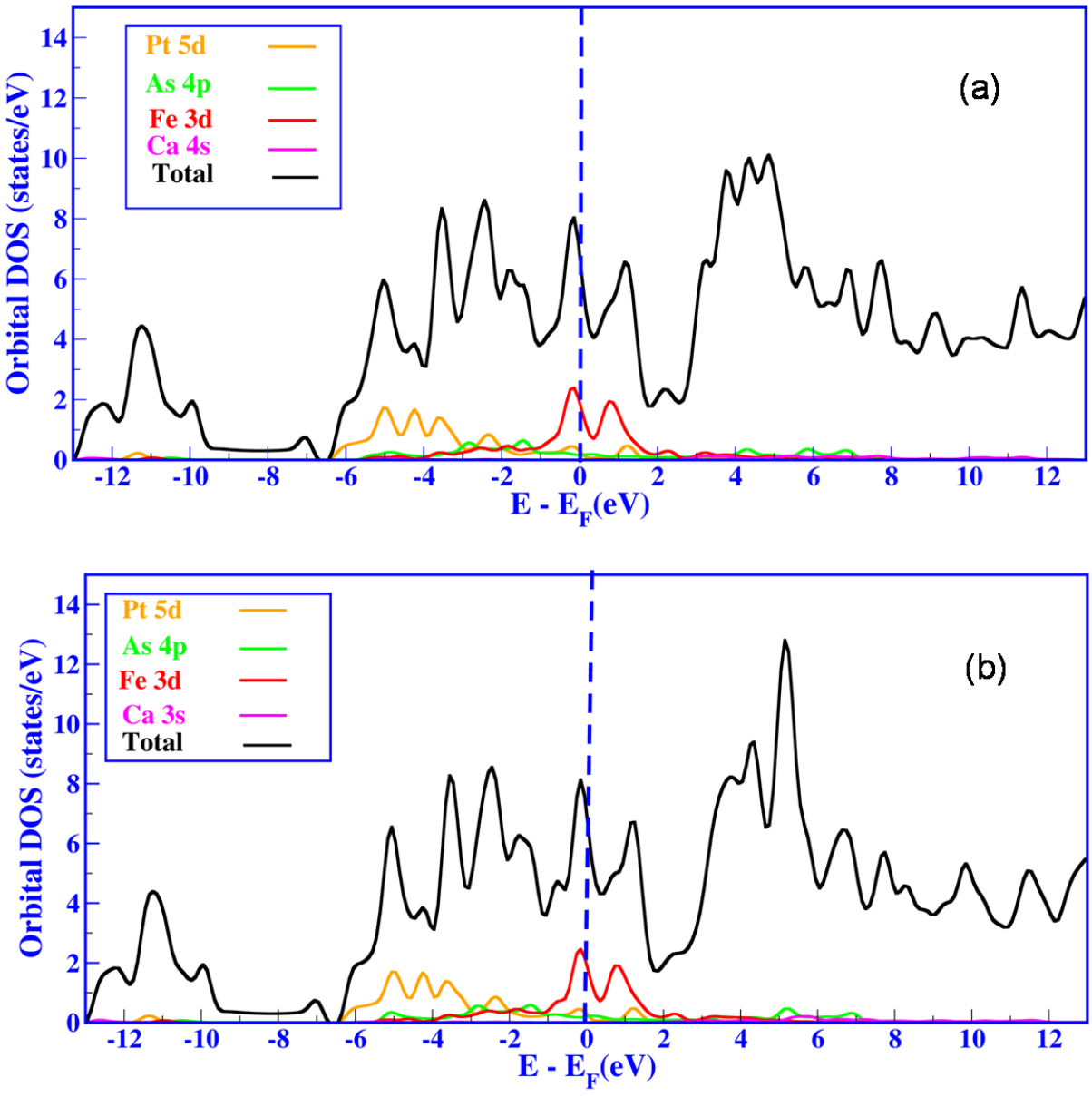

Figure 2.12: Orbital density of states for AFM2 phase (a) type-A (b) type-B

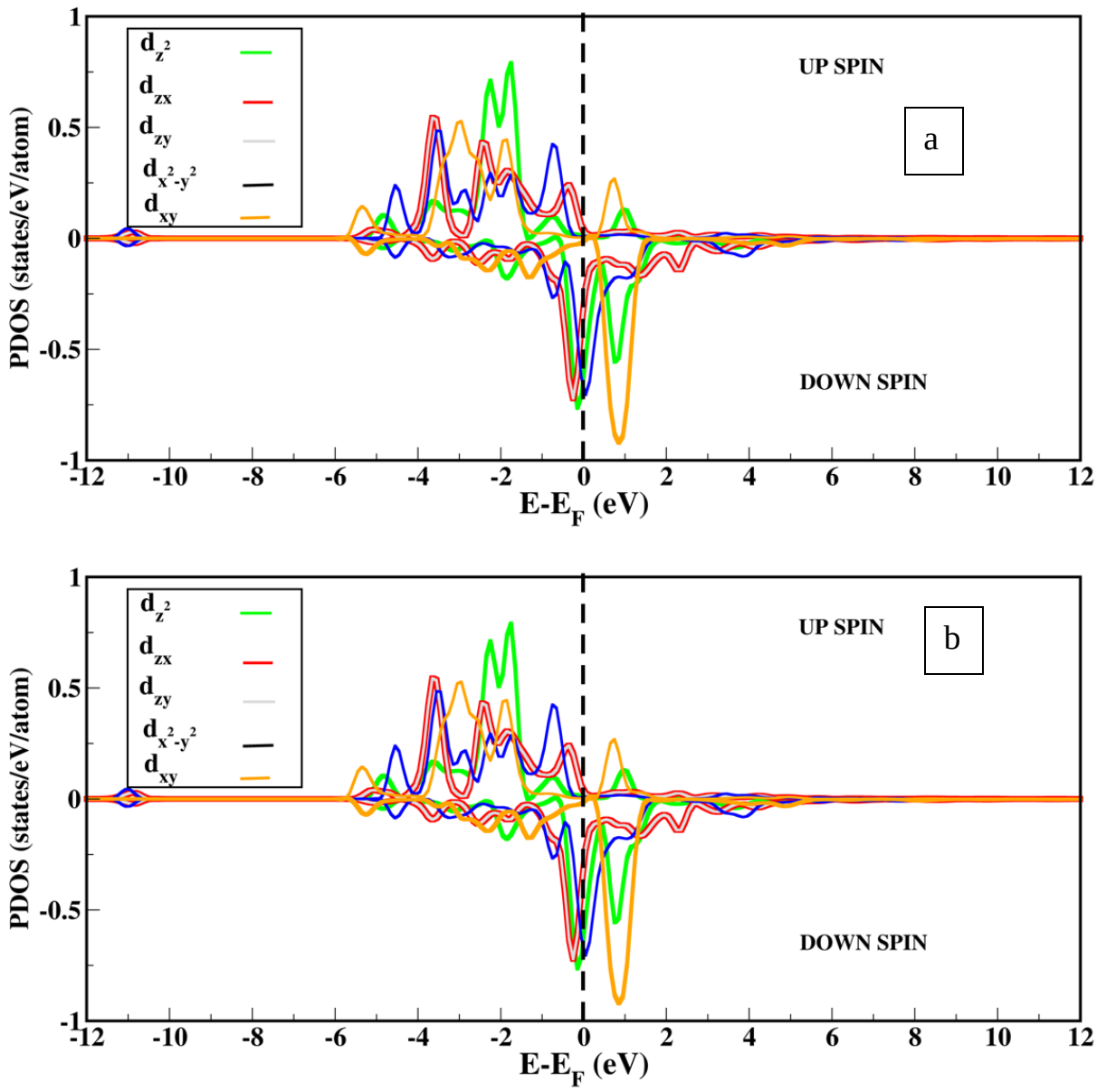

Figure 2.13: contribution of different d orbitals :(a) type-A (b) type-B

Clearly, most of the d orbitals are non-degenerate which gives clear indication of splitting of d orbital's. For type-A structure, spin-up component of d_{zx} and d_{zy} orbital are almost fully filled where as d_{xy} component is partially filled. The splitting of d-orbital is caused by crystal field splitting with tetrahedral local coordination of Fe atoms. Though there is crystal field splitting of Fe '3d' orbitals due to tetrahedral coordination of Fe atoms, d_{zx} and d_{zy} still remain degenerate state in tetragonal symmetry.

2.4 Conclusions

We have systematically investigated the electronic structure of the superconducting system $CaFe_{1-x}Pt_xAs_2$ considering both types of existing crystal structures. Our calculated lattice parameters are in good agreement with experimental value. We find anti ferromagnetic stripe phase (AFM2) to be the ground state among all the other possible spin configurations which are in consistent with various iron-pnictide studies. Due to anti-ferromagnetic magnetic ordering (AFM2), we find anisotropic deformation in the crystal structure. We see the full metallic behavior of the parent compound which is consistent with experimental observation.[17] We find that there is significant overlap between Fe and As orbitals leading to hybridization. The Fe '3d' orbital's contribution is dominant at the Fermi level along with small contribution from As atomic orbitals. Hence Fe-As block plays the major role in the formation of superconductivity. Our calculated band diagram is highly dispersive and bands crossing the Fermi level give rise to electron and hole pocket in the Fermi surface. In the Fermi surface the dispersion along z-direction is quite low, which is quite unusual, interesting and novel in iron-pnictide

studies. We observe the hole pocket at the Z point and electron pocket at the M point in the BZ which exclude the possibility of s_{+-} symmetry of the superconducting order parameter. This finding is well suited with experimental predictions. The electronic structure of both the configurations (type-A and type-B) is similar. As electronic structure is closely related to the critical temperature (T_C), this finding also explains similar T_C values obtained from experiments.

Reference

[62]L.Gao, Y.Y. Xue, F.Chen, Q. Xiaong, R.L. Menge, D. Remirez , C.W.Chu, J.H. Eggert and H.K. Mao, *Phys.Rev. B, 50, 4260-4263 (1994)*

[63]Jun Nagamatsu, Norimasa NaKagawa, Takahiro Muranaka, Yuji zenitani, Jun Akimitsu, *Nature 410, 63, (2001)*

[64] Yasuhiro Takabayashi, Alexey Y. Ganin, Peter Jeglič, Denis Arčon, Takumi Takano,Yoshihiro Iwasa, Yasuo Ohishi, Masaki Takata, Nao Takeshita,8 Kosmas Prassides, Matthew J. Rosseinsky. Science 323, 1586 (2009)

[65] Yoichi Kamihara, Takumi Watanabe, Masahiro Hirano and Hideo Hosono, *J.AM.CHEM.SOC. 130, 3296-3297 (2008)*

[66] Takayuki Kawamata, Takefumi lida, Kazunori Suzuki, Erika SatOmi, Yoshiaki Kobayashi, Masayuki Itoh, and Masatoshi Sato. J.Phys.Soc.Jpn. 80, 073710 (2011)

[67] Kazutaka Kudo, Masakazu Kobayashi, Satomi Kakiya, Masataka Danura, and Minoru Nohara. J. Phys. Soc. Jpn. 81 (2012) 035002

[68] E.Akturk and S. Ciraci , *Phys.Rev. B, 79,184523 (2009)*

[74] Kazuhiko Kuroki, Hidetomo Usui, Seiichiro Onari, Ryotaro Arita, and Hideo Aoki, Phys.Rev.B, 224511 (2009)

[75] F. Ronning, J.-X. Zhu, Tanmoy Das, M.J. Graf, R.C. Albers, H.B. Rhee and W.E. Pickett . arxiv:1203.0579v1

[76] I.I. Mazin, D.J.singh, M.D.Johannes, andM.H. Du, Phys.Rev.Lett.101, 057003(2008)

[8]Johrendt D and Pottgen R *2008 Angew.chem.Int.Edn 47 4782*

[9]M.Rotter,M. Tegel, and D.Johrendt, *phys.Rev.Lett.101, 107006(2008*)

[10]M.Rotter, M.Tegel, D.Johrendt,I.scheelenberg, W.Hermes, and R.Pottegen,*Phys.Rev.B 78,020503(2008)*

[11]D.Kasinathan,A. Ormeci, K.Koch, U.Burkhardt, W. Schnelle, A. Leithe-Jasper, and H.Rosner,*New J. phys. 11,025023 (2009)*

[12]C.krellner, N.Caroca-Canales, A.Jesche, H.Rosner, A.Ormeci, and C.Geibel, *Phys. Rev.B 78,100504(2008)*

[13]M.V. Sadovskii, *Phys. Usp 51.1201(2008)*

[14]A.L. Ivanovskii, *Phys. Usp. 51. 1229 (2008)*

[15]H. Hiramatsu, T. Kamiya, M.Hirano, and H.Hosono, *physica C 469, 657 (2009)*

[16]P.C.Canfield and S.L.Bud'ko, *Annu. Rev. Condense, Matter Phys. 1, 27 (2010)*

[17] Takayuki et al *J. Phys. soc. Japan 80, 073710(2011)*

[18]Kazutaka et al *J.Phys.soc.Japan 81, 035002(2012)*

[19]R.Settai,H. Shishido, S.Ikeda, Y.Murakawa, M. Nakashima, D. Aoki, Y. Haga, H. Harima, and Y.Onuki, *journal of Physics:Condense Matter 13, L627(2001)*

[20]H. Shishido, R.Settai, D.Aoki, S.Ikeda, H. Nawaki, N. Nakamura, T. Iizuka, Y. Inada, K. Sugiayama, T. Takeuchi, K. Kindo, T.C. Kobayashi, Y. Haga, H. Hairma, Y.Aoki, T.Namiki, H. Sato, and Y.Onuki, *J. Phys. Soc. Jpn 71,162 (2002)*

[21] D. Hall, E.C. Palm, T.P. Murphy, S. W. Tozer, Z. Fisk, U.Alver, R.G. Goodrich, J.L. Sarrao, P.G. Pagliuso and T.Ebihara, *Phys.Rev. B 64, 212508 (2001)*

[22] E.Akturk and S. Ciraci , *Phys.Rev B, 79,184523 (2009)*

[23] Baroni S, Dal Corso A, de Gironcoli S and Giannozzi P *2001http://www.pwscf.org*

[24] Vanderbilt D *1990 Phys.Rev.B 41 7892*

[25]http://www.library.cornell.edu/nr/bookcpdf/c10-7.pdf

[26]Methfessel and Paxton A T *1989 Phys.Rev.B 40 3616*

[29]I.I. Mazin, D.J.singh, M.D.Johannes, andM.H. Du, Phys.Rev.Lett.101,057003(2008)

[30]A.V. Chubukov and Z. Tesanovic, Europhys.Lett. 85, 37002(2009)

[31]K.seo, B.A. Bernevig, and J.Hu, *Phys.Rev.Lett. 101, 206404(2008)*

[32]V.Cvetkovic and Z.Tesanovic, *Europhys.Lett. 85, 37002(2009)*

[33]S.Ishibashi, K.Terakura and H. Hoson , *J. Phys. soc. jpn 77, 053709(2008)*

[34]Y.F. Li, L.F. Zhu, S.D.Guo, Y.C.Xu and B.G. Liu, *J.Phys.Condens. Matter 21, 115701 (2009)*

[35]F. Ronning, J.-X. Zhu, Tanmoy Das, M.J. Graf, R.C. Albers, H.B. Rhee and W.E. Pickett arxiv:1203.0579v1

[36]Yin Z P, Lebegue S, Han M J, Neal B P, Savrasov S Y and pickett W E 2008 *Phys.Rev.Lett.101 047001*

Chapter 3

First-Principles Analysis on Structural Transition in $BaNi_2As_2$ Superconductor

3.1 Introduction

The discovery of superconductivity with transition temperature (T_C) 56K in $RFeAsO_{1-x}F_x$ (R=Sm, Nd, Pr…) [1-6] has attracted attention of many researchers to understand the superconducting mechanism. Besides, the appearance of superconductivity in Ni-based compounds which posses low T_C,i.e., LaONiP (T_C=3K)[7], LaONiAs(T_C=2.75 K)[8], $BaNi_2P_2$ (T_C=2.4 K)[9], $BaNi_2As_2$ (T_C=0.7 K)[10] and $SrNi_2As_2$ (T_C=0.62 K)[11] give a new platform to understand the microscopic reasons behind such phenomenon. Hence it is important to understand why T_C is low in Ni-based compounds, which may enrich our understanding about the high T_C in iron-based superconductors. The high T_C in superconductors is sometime associated with structural instability. It has been reported that there is an increase in T_C at structural phase boundary in various systems including cuprates [12, 13], iron-pnictide superconductors [14, 15], A15 compounds [16], graphite intercalated compounds and elements including Li and Te under high pressure [17-19].

Among all the Ni-based pnictides, $BaNi_2As_2$ is mainly important because it is regarded as a non-magnetic analogue of iron-based superconductors e.g $CaFe_2As_2$. Besides these similarities, there

is some dissimilarity too. It is reported that collinear spin-density-wave magnetic ordering does not exist in $BaNi_2As_2$ [20]. The absence of magnetism may be one of the reasons for low T_C in $BaNi_2As_2$ [21-24]. This clearly indicates the importance of magnetism in iron-pnictide superconductors for its high T_C. $BaNi_2As_2$ has the following properties: (1) It is observed that structural phase transition is first-order in $BaNi_2As_2$ [25]. (2) It is predicted that band-shift in $BaNi_2As_2$ is due to considerable lattice distortion. (3) Correlation effect in BaNi2As2 is very weak since small band renormalization factor in $BaNi_2As_2$. Very recently, it is reported that the structural phase transition in $BaNi_2As_2$ can be tuned by phosphorus doping [33]. Pressure-induced structural phase transition in this system is particularly interesting since it can provide a new way for finding the reason behind the mechanism of high-temperature superconductivity. Based on this interesting report, in this work, we present a first-principle study of $BaNi_2As_2$. Our approach reproduces and explains the experimentally observed changes in T_C with pressure and establishes the relation between the sudden jump in T_C and the structural phase transition. In addition, we address the following questions: (a) how does lattice parameter depend on doping concentration? (b) What is the reason behind doping induced lattice distortion? (c) Is increase in the superconductivity in the tetragonal phase electronic or is it phonon mediated?

3.2 Computational details

Correlation effect in $BaNi_2As_2$ is very low because of small band renormalization factor [20]. Hence non-interacting density functional theory is appropriate in this context. All calculations are performed by considering pseudo potential-based density functional theory (DFT) as implemented in the PWSCF package [61]. We consider generalized gradient approximation (GGA) [62] for the exchange correlation function and use ultra-soft pseudo potential for taking into account the interaction between the ion's core and the valance electrons. We take 3×3×1 super cell for the simulation of $BaNi_2$ $(As_{1-x}P_x)_2$ with x=0.0, 0.027, 0.055, 0.083, 0.11. Optimization is done with respect to both atomic position and lattice-parameters using Broyden-Fletcher-Goldfarb-shanon (BFGS) method. Plane-wave basis is used with a kinetic energy cutoff of 40 Ry for wave functions and cutoff of 400 Ry for charge density. For the integration over the Brillouin Zone of 3×3×1 super cell containing 90 atoms, we take 3 ×3× 3 Monkhorst-Pack mesh [63]. Convergence is checked carefully in wave-vector space and considered by taking the energy difference between two consecutive steps, 10^{-8} Ry. Spin polarized calculation is neglected in all calculation since there is no existence of spin ordering in $BaNi_2As_2$.

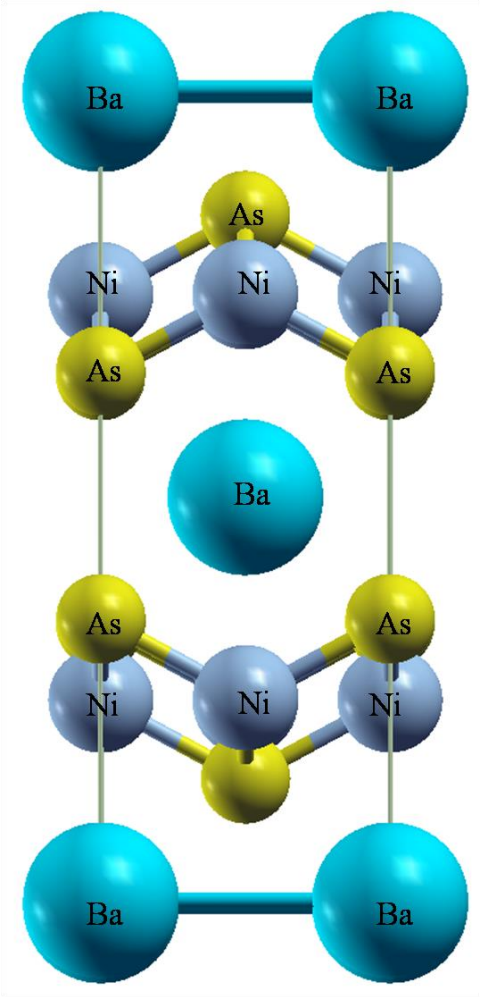

Figure 14 Crystal structure of $BaNi_2As_2$

Table 5 Data for structural parameter and atomic position for the unit cell of $BaNi_2As_2$ at 297 K

Reference	Lattice parameter a(Å)	Lattice parameter c(Å)	Z_{As}
this work	4.192	11.231	0.349
Earlier work[34]	-	-	0.351
Expt.[33]	4.147	11.619	0.347

3.3 Results and discussion

The unit cell of $Bi_2Ni_2As_2$ at T=293K has the tetragonal structure with I4/mmm symmetry. To verify our structure of $Bi_2Ni_2As_2$, we do variable cell optimization of the unit cell and compare the unit cell parameters of $BaNi_2As_2$ with earlier findings and experimental structure as shown in Table1. Our calculated lattice parameters 'a' and 'c' of the unit cell are 1% larger and 3.3% smaller than experimental values [33] respectively. Our computed Z_{As} (height of the As atom from the bottom of the unit cell) is in good agreement with earlier work [34] with 0.5% smaller value but 0.5% larger than the experimental one [33]. The calculated lattice constants and atomic positions of the unit cell are used as initial values in the super-cell calculations. To explore the pressure dependence on the structure, we do the calculation with various doping concentrations (0.0, 0.027, 0.055, 0.083, 0.11) as described in experimental study [33].

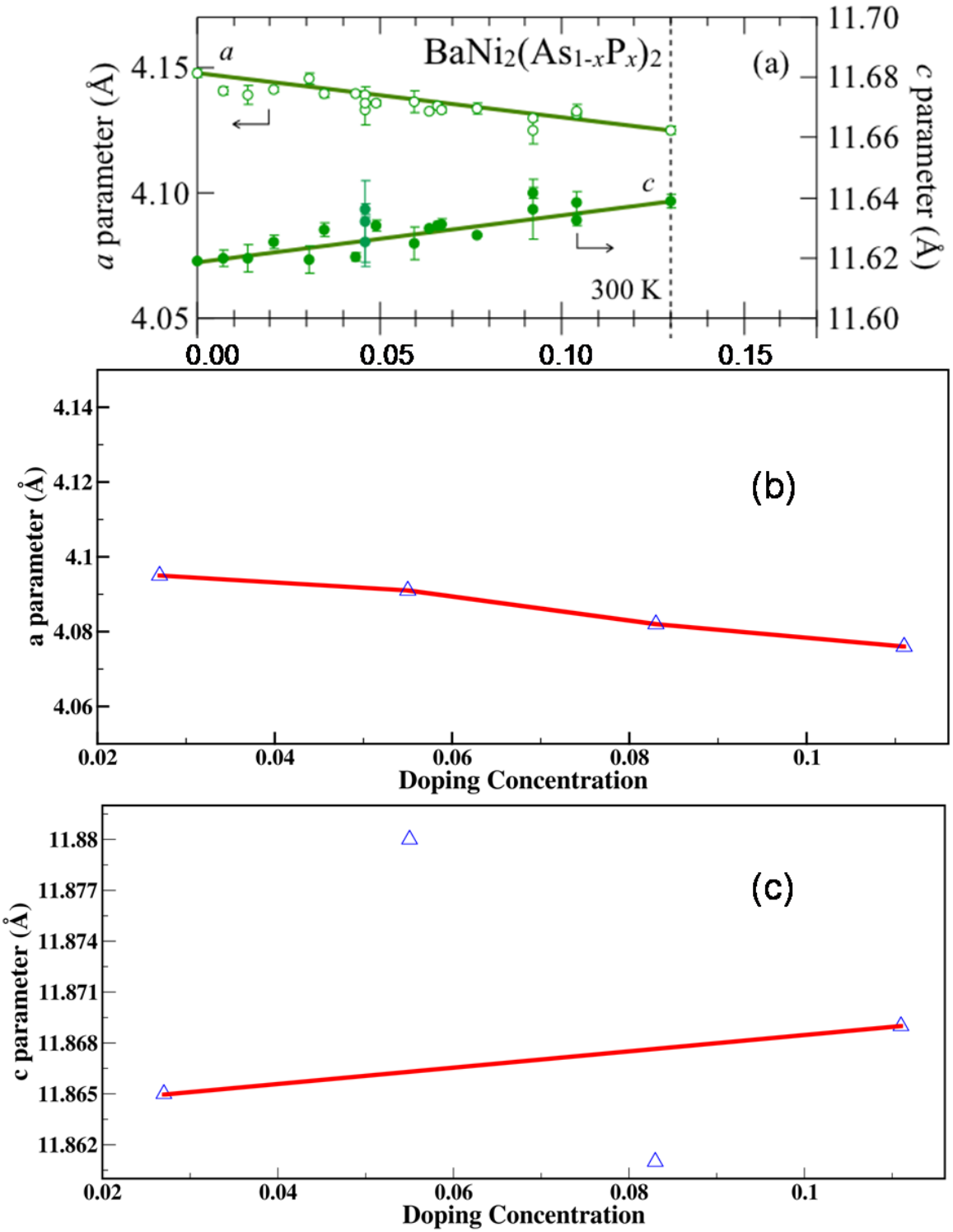

Figure 15 (a) Lattice parameters a and c as a function of phosphorous content x for $BaNi_2(As_{1-x}P_x)_2$ as predicted by experiment [33] (b) calculated dependence of latiice parameter a with various doping concentration (c) calculated dependence of lattice parameter c with various doping concentration

The dependence of lattice parameters ‘a’ and ‘c’ with various doping concentration is plotted in figure 2. We observe that the lattice parameter ‘a’ decreases with increase in doping concentration but lattice parameter ‘c’ increases with increase in doping concentration. This correlation between lattice parameters and doping concentration is in good agreement with experimental one as shown in figure 2 (a). We also predict the decrease of volume with doping as proposed by the experiment [33]. According to our calculations, decrease in volume is 1.7 $Å^3$ with 11% phosphorous doping whereas experiments predicted decrease in volume as 1.1$Å^3$ with 13% phosphorous doping. Given the theoretical approximations, we believe our theoretical results are in reasonable agreement with experimental predictions. The origin of pressure dependence of the volume is as follows: the valance electrons of phosphorous and arsenic are same. But the ionic radius of phosphorous is smaller than arsenic. When we substitute arsenic by phosphorous, this doping creates chemical pressure. That is why; we find this kind of monotonic dependence of lattice parameters with doping concentration and overall volume of the cell. As shown in figure 3(a), with the increase in doping concentrations, energy increases. In other words, doping creates the instability in the structure and the structure tends to go to other phase for stability. From figure 3(b), it is clear that with the increase in doping concentration, the pressure increases. We see structural distortion due to this pressure which appears due to the application of doping. From figure 3 (b), it is interesting to observe that within doping concentration between 0.02 and 0.05 pressure almost increases linearly and in between 0.07 and 0.11 pressure decreases linearly. But in the region between 0.06 and 0.07, pressure remains almost constant. That means, up to doping concentration 0.05, structure becomes unstable in one phase in which it exists. Beyond the range of 0.05, it starts going to another phase. After doping

concentration of 0.065, it reaches in one new phase in which it is again stabilizes as pressure decreases.

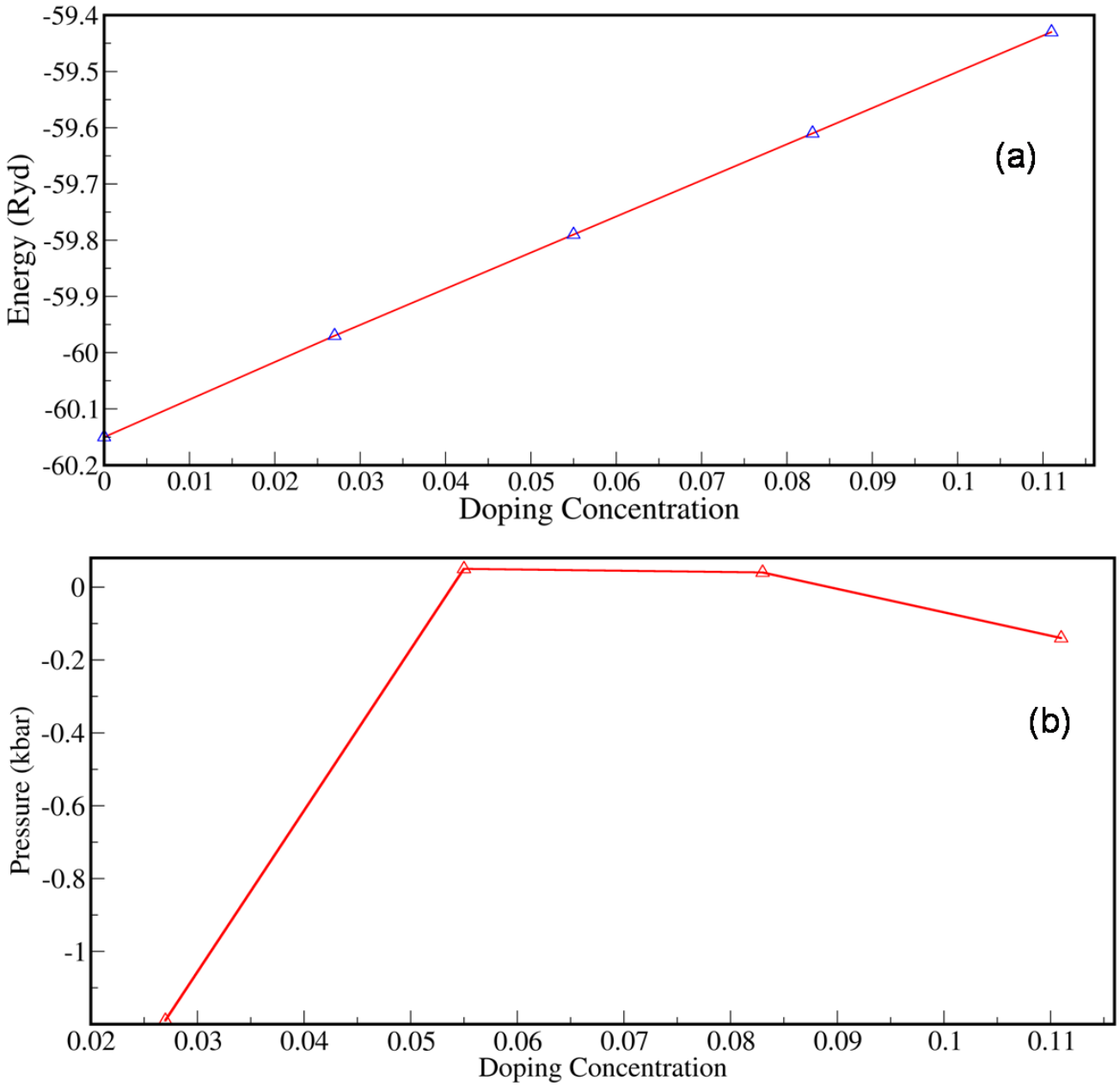

Figure 16 (a) Energy variations with various doping concentrations (b) variation of pressure with various doping concentrations

In between 0.06 and 0.07 doping concentrations, pressure remains almost independent of doping concentration. So we can think of structural phase transition occuring in between 0.06 and 0.07 doping concentrations. In fact, experimentally it is observed that the structural phase transition occurs at the doping concentration, 0.067. With the application of doping, besides the lattice parameters, internal parameters also change. This is shown in figure 4. In figure 4, it is clearly seen the bond angle, < Ni-As-Ni, changes with the increase in doping concentration. But it is again interesting to note that there is sudden jump in the change of the bond angle in between doping concentration 0.06 and 0.07. This suggests that the structural phase transition occurs somewhere between doping concentration 0.06 and 0.07 which is in good agreement with experimental findings [33].

Table 6 Data for density of states $N(E_F)$ at the Fermi level with various doping concentrations

Reference	Doping concentration	$N(E_F)$ $(eV)^{-1}$
This work	0.00	7.18
Expt.[33]	0.00	6.00
Singh et al.[34]	0.00	7.14
This work	0.25	7.19
Expt.[33]	0.25	6.00

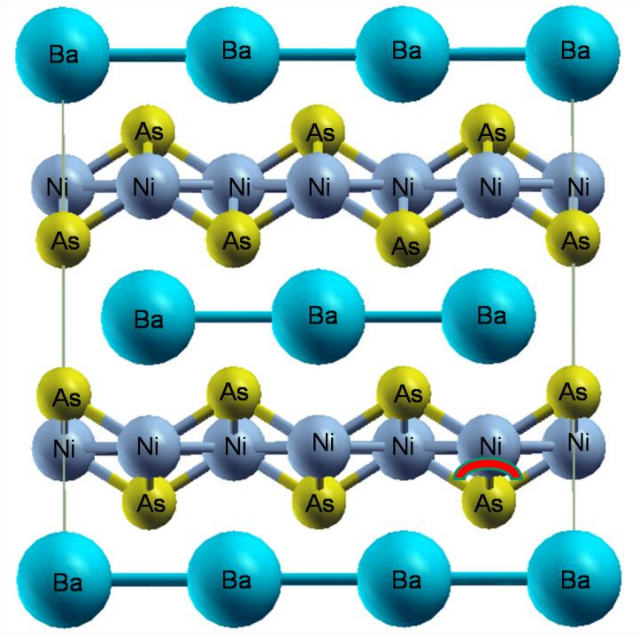

Figure 17 3× 3×1 super cell of $BaNi_2(As_{1-x}P_x)_2$

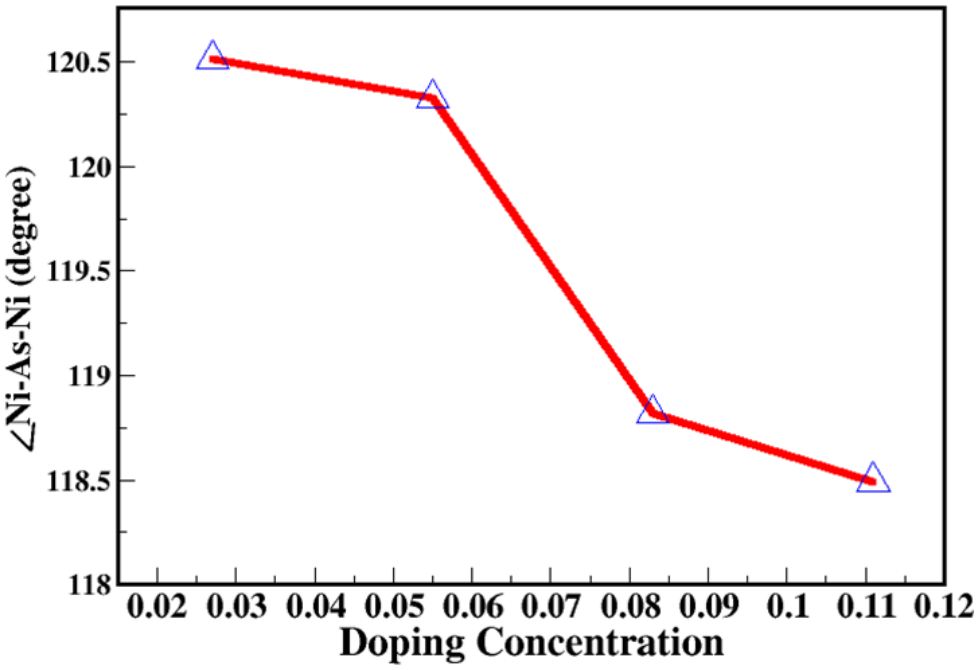

Figure 18 Change in the bond angle with doping concentration

Thus, there is structural phase transition in $BaNi_2(As_{1-x}P_x)_2$ due to the application of doping. With this structural phase transition, there is increase in T_C which is the main advantage of this transition. Now the question is what is the origin of this enhancement in the value of T_c? Is it related with electron or phonon? To find out the reason, we have plotted density of states (DOS) in various doping concentrations which is shown in Fig. 6. There is finite density of states at the Fermi level in both doping concentration (x=0.0 and x=0.25). So the parent composition, $BaNi2(As_{1-x}P_x)_2$, superconductor is metallic like iron-pnictide superconductors and this metallic behavior of $BaNi_2(As_{1-x}P_x)_2$ is independent of the amount of doping. From the DOS at x=0.0 doping concentration, we have computed the density of state at the Fermi level, N (E_F), which is in good agreement with earlier work and experimental prediction. All these values are tabulated in Table 2. We have also calculated N (E_F) for the higher doping concentration. This N (E_F) value for the higher doping concentration (x=0.25) is also in agreemant with experimental value. Interestingly, calculated values of N(E_F) are independent of the doping concentrations.

$$\gamma = \frac{\pi^2}{3} N(E_F) k_B^2 \qquad (3.1)$$

Where γ is the electronic specific heat coefficient, k_B is the Boltzmann constant and N(E_F) is the density of state at the Fermi level.

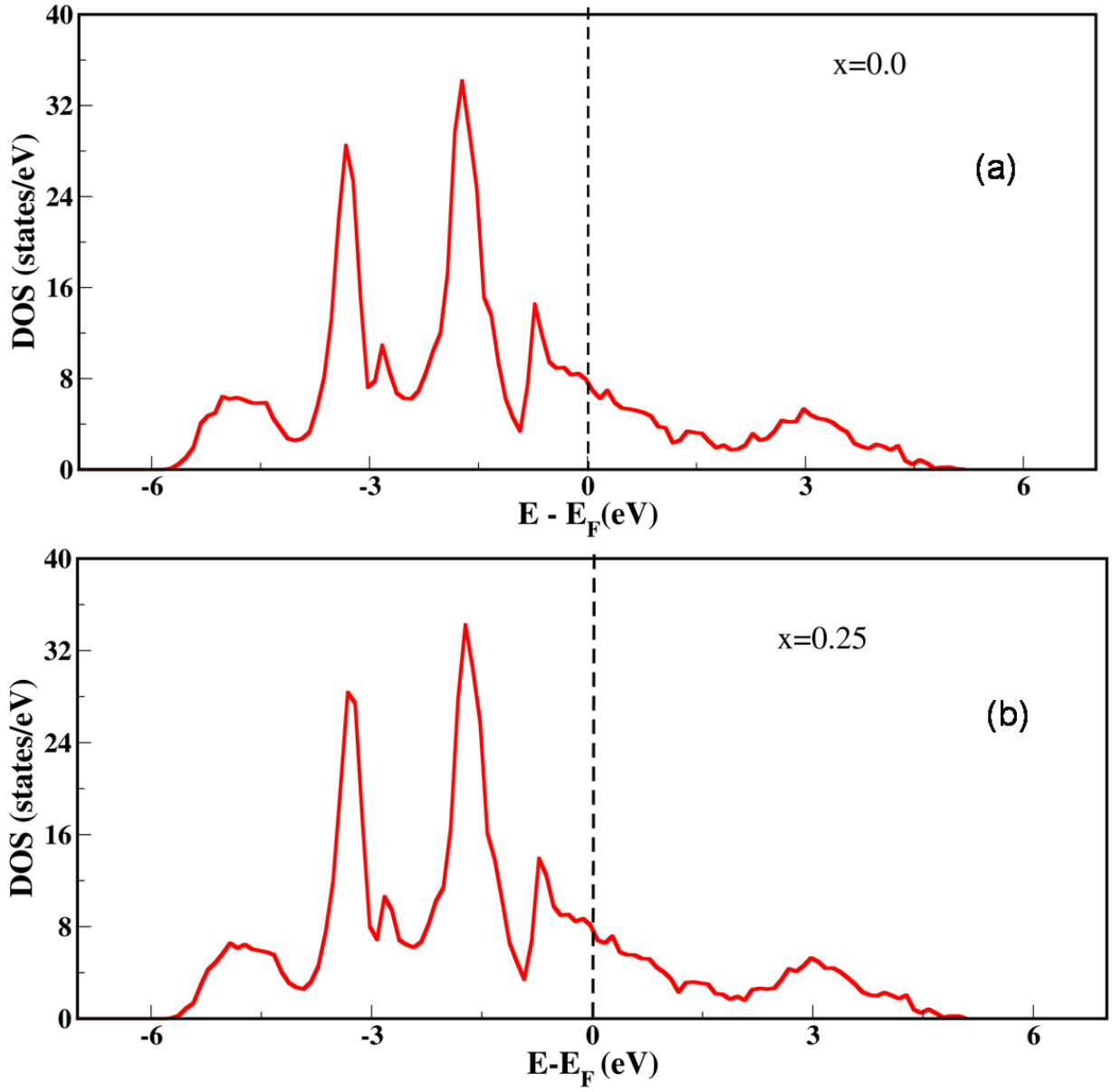

Figure 19 Density of state plot for various doping concentrations (a) 0.00 (b) 0.25

$$\gamma^{expt} = \gamma^{theor}(1+\lambda_{ep}) \tag{3.2}$$

Where λ_{ep} is the electron-phonon coupling constant.

$$k_B T_c = \frac{\hbar\omega_{ln}}{1.2}\exp\{-\frac{1.04(1+\lambda_{ep})}{\lambda_{ep}-\mu^*(1+0.62\lambda_{ep})}\} \tag{3.3}$$

Where ω_{ln} is the logarithmic average of phonon frequency and μ^* is a constant and equal to 0.12

From equation (3.1), it is clear that electronic specific- heat coefficient (γ) is directly related with $N(E_F)$. Basically, it is only a function of $N(E_F)$ within free electron theory. Now, if $N(E_F)$ is independent of the amount of doping, the value should be remain constant with doping. This explains the experimental prediction of the variation of specific heat with temperature. According to experimental observations, the slope of the C/T vs. T^2 plot is almost unchanged with various doping concentration. This indicates the independent value of electronic specific-heat coefficient (γ) with various doping concentrations. From equation (3.2), electron-phonon coupling constant is roughly related with γ . If γ is constant against doping concentration, then electron-phonon coupling is also constant with various doping concentration. From Allen-Dynes formula, as given in equation (3.3), it is clear that transition temperature is a function of logarithmic average of phonon frequency ω_{ln} and electron-phonon coupling constant λ_{ep} . Now if λ_{ep} remains almost constant with various doping concentrations, then the only possibility for the increase in transition temperature (T_C) is ω_{ln} . Hence, the enhancement in T_C is related with

phonons, not with electrons. Our finding for the origin of the enhancement in the superconductivity is in complete agreement with the experimental predictions.

3.4 Conclusion

We have presented a systematic first-principles study on the structural phase transition in $BaNi_2(As_{1-x}P_x)_2$ superconductor. Our calculated dependence of lattice parameters with various doping concentrations is in well agreement with experimental findings. We have also found overall decrease in volume with increase in the doping concentrations, which compares fairly well with experimental findings. We have seen distortion in the internal parameters like bond angle (<Ni-As-N) changes significantly with increase in the doping concentrations. We have clearly found the reasons behind the crystal distortions with doping. We have shown phosphorous doping creates pressure on $BaNi_2(As_{1-x}P_x)_2$ and how this induced pressure produces instability in the system. We have predicted the enhancement in the increase of transition temperature (T_C) is related with phonons not with electrons.

References:

(1)Z.A.Ren, W.Lu, J.Yang, W.Yi, X.-L. Shen, Z.Cai, G-c. Che, X.-L. Dong, L.-L. Sun, F.Zhou, and Z.-X. Zhao, *Chin.Phys.Lett. 25, 2215 (2008)*

(2)R.H. Liu, G. Wu, T. Wu, D. F. Fang, H.Chen, S.Y. Li, K. Liu, Y.L.Xie, X.F. Wang, R.L. Yang, L. Ding, C. He, D.L. Feng and X.H. Chen,*Phys.Lett.101, 087001 (2008)*

(3)Chunlei Wang, Zhaoshun Gao, Lei wang, Yanpeng Qi, Dongliang Wang, Chao Yao, Zhiyu Zhang, and Yanwei Ma, *Supercond.Soc. Technol.23, 055002(2010)*

(4)Zhi-An Ren, Jie Yang, Wei Lu, Wei Yi, Xiao-Li-shen, Zheng-Cai Li, Gaung-Can Che, Xiao-Li Dong, Li-Ling Sun, Fang Zhou, and Zhong-xian Zhao, *EPL 82,57002 (2008)*

(5)A. Kursumovic, J. H. Durrel, S. K. Chen, and J.L. MacManus-Driscoll, *supercond. Sci. Technol. 23, 025022 (2010)*

(6)Z.A. Ren, J.Yang, W. Lu, W.Yi, G.C. Che, X.L. Dong, L.L. Sun, and Z.X. Zhao, *Material Research Innovations 12,105, (2008)*

(7)Takumi watanabe, Hiroshi Yanagi, Toshio Kamiya, Yoichi kamihara, Hidenori Hiramatsu, Masahiro Hirano, and Hideo Hosono, *Inorg. Chem. 46, 7719 (2007)*

(8) Zheng Li, Gengfu chen, Jing Dong, Gang Li, Wanzheng Hu, Dan Wu, Shaokui Su, Ping zheng, Tao xiang, Nanlin wang, and Jianlin Luo, *Phys.Rev. B 78, 060504(R) (2008)*

(9)Y.Tomioka, S. Ishida, M.Nakajima, T.ito, H. Kito, A.Iyo, H. Eisaki, and Suchida, Phys.Rev.B 79, 132506(2009)

(10)F. Ronning, N. Kurita, E.D. Bauer, B.L.scott, T.Park, T.Klimczulk, R. Movshovich, and J.D. Thpmpson, J. Phys.Condense. Matter 20, 342203 (2008)

(11)

(12) M. d'Astuto, P. K. Mang, P. Giura, A. Shukla, P. Ghigna, A.Mirone, M.Braden, M. Greven, M.Krisch and F.Sette, Phys. Rev. Lett.88, 167002 (2002)

(13) D. Reznik, L. Pintschovius, M. Ito, S. Iikubo, M. Sato, H. Goka, M. Fujita, K. Yamada, G.D. Gu and J.M. Tranquada, Nature 440, 1170 (2006)

(14) T. Goto, R. Kurihara, K. Araki, K. Mitsumoto, M. Akatsu, Y. Nemoto, S. Tatematsu and M. Sato, J. Phys. Soc. Jpn. 80, 073702 (2011)

(15) M. Yoshizawa, D. Kimura, T. Chiba, S. Simayi, Y. Nakanishi, K. Kihou, C.-H. Lee, A.Iyo, H. Eisaki, M. Nakajima and S. Uchida, J. Phys. Jpn. 81, 024604 (2012)

(16)L.R. Testardi, Rev. Mod. Phys. 47, 637 (1975)

(17) R. P. Smith, A. Kusmartseva, Y. T. C. Ko, S. S. Saxena, A. Akrap, L. Forr, M. Laad, T.E. Weller, M. Ellerby and N. T. Skipper, Phys. Rev. B, 74, 024505 (2006)

(18) J. S. Kim, L. Boeri, R. K. Kremer, and F. S. Razavi, Phys. Rev. B, 74, 214513 (2006)

(19) A. Gauzzi, S. Takashima, N. Takeshita, C. Terakura, H. Takagi, N. Emery, C. Herold, P. Lagrange and M. Hanfland and M. Mezouar, Phys. Rev. B, 78, 064506 (2008)

(20) Bo Zhou, Yan Zhang, Le-Xian Yang, Min Xu, Cheng He, Fei Chen, Jia-Feng Zhao, Hong-Wei Ou, Jia Wei, Bin-Ping Xie, Tao Wu, Gang Wu, Masashi Arita, Kenya Shimada, Hirofumi Namatame, Masaki Taniguchi, X. H. Chen, and D. L. Feng, Phys. Rev. B 83,035110, (2011)

(21) A. J. Drew, Ch. Niedermayer, P. J. Baker, F. L. Pratt, S. J. Blundell, T. Lancaster, R. H. Liu, G. Wu, X. H. Chen, I. Watanabe, V. K. Malik, A. Dubroka, M.Rössle, K. W. Kim, C. Baines, and C. Bernhard, Nat. Mater. 8, 310 (2009).

(22) A. D. Christianson, E. A. Goremychkin, R. Osborn, S. Rosenkranz, M. D. Lumsden, C. D. Malliakas, I. S. Todorov, H. Claus, D. Y. Chung, M. G. Kanatzidis, R. I. Bewley, and T. Guidi, Nature 456, 930 (2008).

(23) L. Ma, J. Zhang, G. F. Chen, and Weiqiang Yu, Phys. Rev. B 82, 180501(R) (2010).

(24) S. Graser, A. F. Kemper, T. A. Maier, H. P. Cheng, P. J. Hirschfeld, and D. J. Scalapino, Phys. Rev. B 81, 214503 (2010)

(25) Athena S. Sefat, Michael A. McGuire, Rongying Jin, Brian, C. Sales, David Mandrus, Filip Ronning, E. D. Bauer, and Yurij Mozharivskyj, Phys. Rev. B 79, 094508 (2009)

(26) C. He, Y. Zhang, B. P. Xie, X. F. Wang, L. X. Yang, B. Zhou, F. Chen, M. Arita, K. Shimada, H. Namatame, M. Taniguchi, X. H. Chen, J. P. Hu, and D. L. Feng, Phys. Rev. Lett. 105, 117002, (2010)

(27) M. Yi, D. H. Lu, J. G. Analytis, J.-H. Chu, S.-K. Mo, R.-H. He, M. Hashimoto, R. G. Moore, I. I. Mazin, D. J. Singh, Z. Hussain, I. R. Fisher, and Z.-X. Shen, Phys. Rev. B 80, 174510 (2009)

(28) Y. Zhang, J. Wei, H. W. Ou, J. F. Zhao, B. Zhou, F. Chen, M. Xu, C. He, G. Wu, H. Chen, M. Arita, K. Shimada, H. Namatame, M. Taniguchi, X. H. Chen, and D. L. Feng, Phys. Rev. Lett. 102, 127003 (2009).

(29) L. X. Yang, Y. Zhang, H. W. Ou, J. F. Zhao, D. W. Shen, B. Zhou, J. Wei, F. Chen, M. Xu, C. He, Y. Chen, Z. D. Wang, X. F. Wang, T. Wu, G. Wu, X. H. Chen, M. Arita, K. Shimada, M. Taniguchi, Z. Y. Lu, T. Xiang, and D. L. Feng, Phys. Rev. Lett. 102, 107002 (2009)

(30) Bo Zhou, Yan Zhang, Le-Xian Yang, Min Xu, Cheng He, Fei Chen, Jia-Feng Zhao, Hong-Wei Ou, Jia Wei, Bin-Ping Xie, Tao Wu, Gang Wu, Masashi Arita, Kenya Shimada, Hirofumi Namatame, Masaki Taniguchi, X. H. Chen, and D. L. Feng, Phys. Rev. B 81, 155124 (2010) .

(31) G.-D. Liu, H.-Y. Liu, L. Zhao, W.-T. Zhang, X.-W. Jia, J.-Q. Meng, X.-L. Dong, J. Zhang, G. F. Chen, G.-L. Wang, Y. Zhou, Y. Zhu, X.-Y. Wang, Z.-Y. Xu, C.-T. Chen, and X. J. Zhou, Phys. Rev. B 80, 134519 (2009).

(32) Bo Zhou, L. X. Yang, Fei Chen, Min Xu, Tao Wu, Gang Wu, X. H. Chen, and D. L. Feng, J. Phys. Chem. Solids. (to be published)

(33) K. Kudo, M. Takasuga, Y. Okamoto, Z. Hiroi, and M. Nohara, arXiv:1204.4958v1 [cond-mat.supr-con]

(34) Alaska Subedi and David J. Singh, Phys. Rev. B, 78, 132511 (2008)

Chapter 4

A study on the surface states of a topological insulator: Bi_2Se_3

4.1 Introduction

The recent discovery of topological insulators opens up a new direction in condensed-matter physics [1, 2]. Topological insulator is a new class of material, in which its bulk is insulating while its surface states are conducting. It is different from ordinary semiconductor in the sense that surface states of topological insulator are robust against any external perturbation because these surface states are protected by time-reversal symmetry [3-5]. The response of surface states to any external perturbations bears great importance for the device applications in spintronics and to discover the new physics at the surface states of topological insulators.

Many binary and ternary chalcogenide compounds, for example, Sb_2Te_3 and Bi_2Se_3 have been discovered and predicted to be topological insulators [6-12]. Among these, Bi_2Se_3 is

expected to be most promising candidate for its application. Its bulk band gap value is quite large and it can go up to 0.3 eV which is higher than the room temperature. Its band inversion occurs at Γ point, providing a simple band structure of the topological surface states with only single Dirac cone. The single Dirac cone can provide us a way to demonstrate the Berry phase which is originating from the spin-momentum locking pattern of the topological surface states that obey time-reversal symmetry. Many exciting phenomena, like, Majorana fermion, topological magneto-electric effects, quantized anomalous Hall effect, have been predicted. All these phenomena need opening of a gap at the Dirac point of the topological surface states. Although the gapless dispersion of the surface states is protected by the time reversal-symmetry, opening up of a gap violate the time reversal-symmetry. One of the easiest ways to break this time reversal symmetry is the application of magnetic doping which can open up a gap opening at the Dirac point [13-15]. So it is expected that surface perturbation can induce a band bending [16, 17]. This kind of band bending can anchor two-dimensional electron gas systems [16], which could show Rashba spin splitting [18]. Already, many studies have been devoted to test the surface states of Bi_2Se_3 and verified that the nontrivial surface state is particularly robust against different kinds of adsorbates [19-21]. But, in device application, the most important test is the response of the topological insulator surface state in ambient conditions. It has been already shown that oxygen can induce a p type doping [22], but the effect of moisture in the air or water vapor still is in mystery. To fulfill this gap in the surface state study of Bi_2Se_3, Benia et al [23] have come up with an experimental study describing the effect of water vapor

on the surface states of Bi_2Se_3. Motivated by this experiment, in this chapter we have addressed the following question to explore the new physics of surface states of Bi_2Se_3: How and why do the water molecules interact with Se surface?

4.2 Computational details

All calculations have been carried out using plane-wave based density functional theory (DFT) method as implemented in the PWSCF package [62]. The interactions between core electrons and valance electrons are approximated by ultrasoft pesudopotentials [63]. The exchange-correlation interaction of electrons is considered within the generalized gradient approximation (GGA) of Perdew-Burke-Ernzerhof (PBE) type [64] . Plane-wave basis sets are used with an energy cut off 30 Ryd for wave functions and a cut off 300 Ryd for the charge density. For the integration over the Brillouin zone, we consider 3× 3×1 Monkhorst Pack Mesh [64].The atomic relaxation is carried out by energy minimization using forces on each of the atoms in the Broyden-Flecher-Goldfarb-Shanno (BFGS) method. Convergence of structure optimizations is obtained considering total energy difference between two consecutive steps less than 10^{-8} Ryd, the maximum force allowed on each atom is less than 10^{-3} Ryd/Bohr.

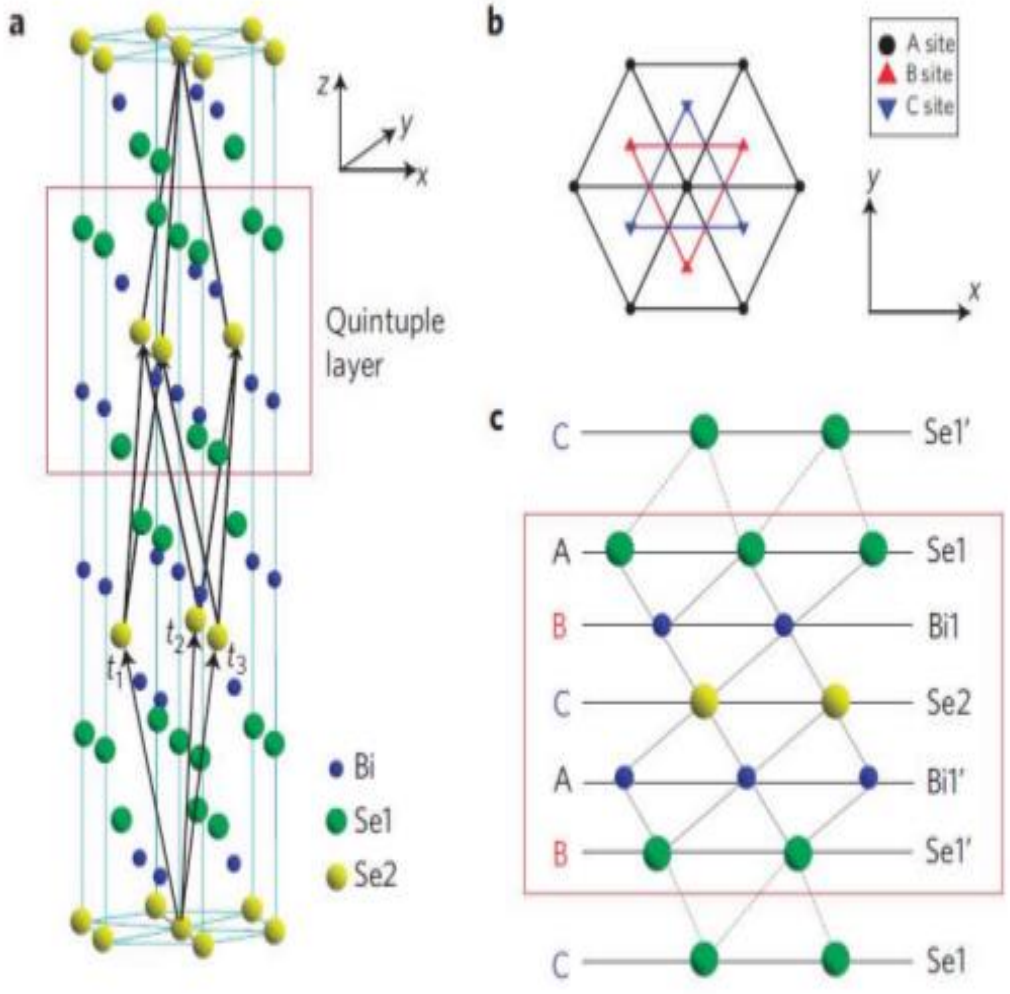

Figure 4.20. Crystal structure of Bi_2Se_3 [12]

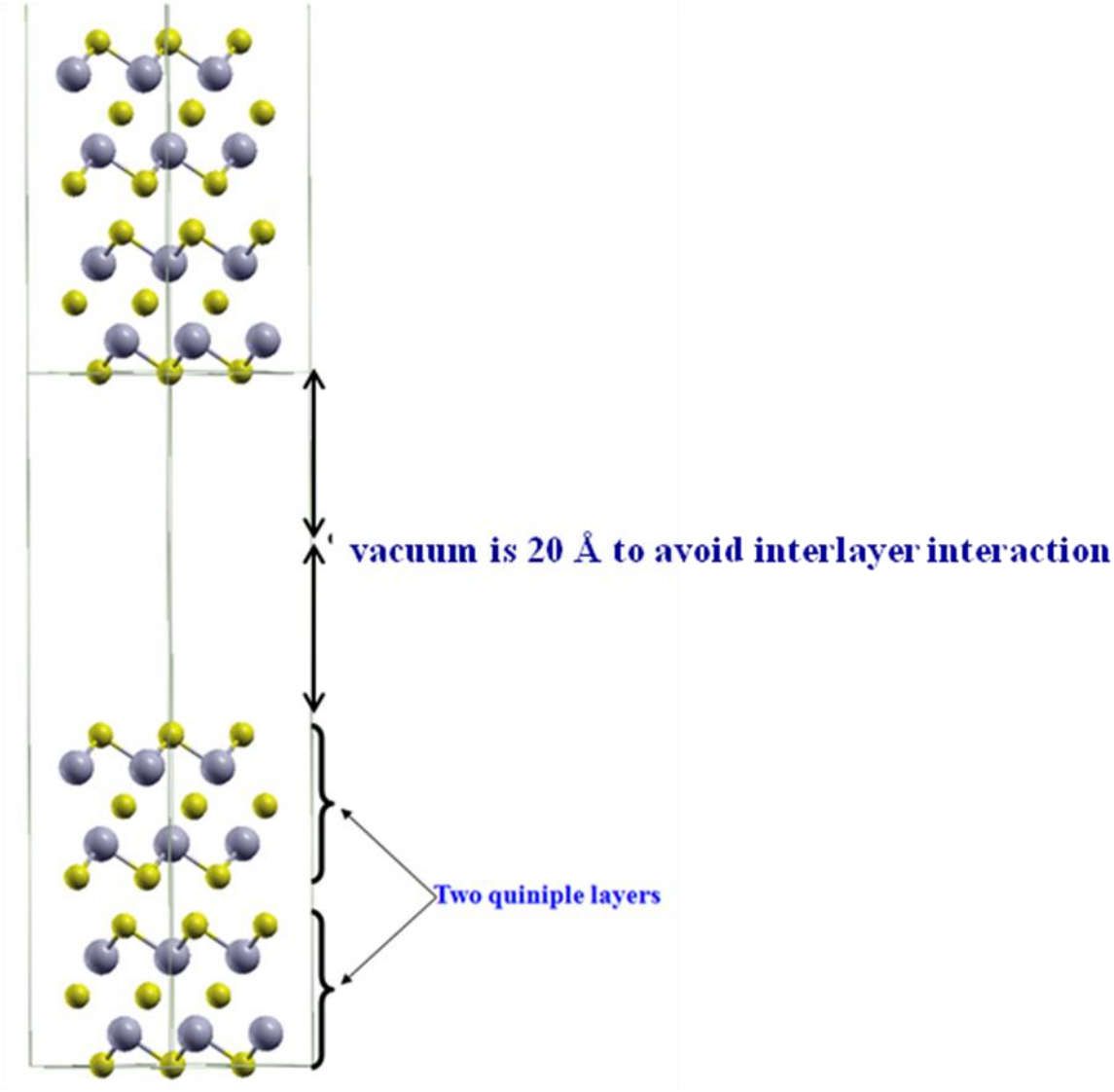

Figure 4.21. Slab geometry of Bi_2Se_3

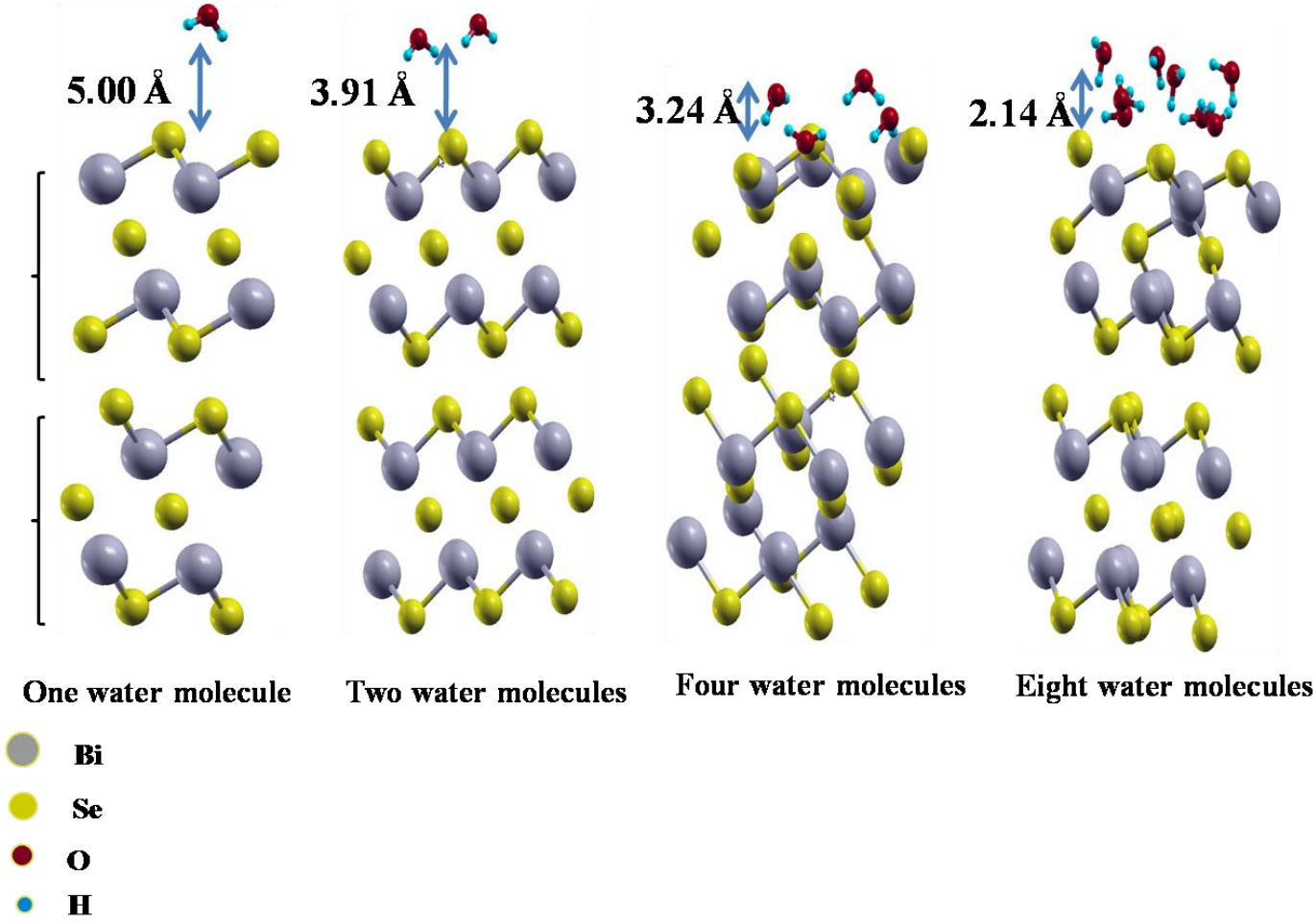

Figure 4.22. Water adsorption on the surface of Bi_2Se_3

4.3 Results and Discussion

The unit cell of Bi_2Se_3 is rhombohedral with space group $D_{3d}^{5}(R\vec{3}m)$ with five atoms in one unit cell. It has layered structure and there is a triangular lattice within each layer (see Fig. 4.1). Z axis can be defined as trigonal axis which has three-fold rotation symmetry, X axis is a binary axis with two fold rotational symmetry and Y axis is bisectrix axis which is in the reflection plane. There are five atoms layers arranged along Z direction. These layers are called quintuple layers. There are five atoms with two equivalent Se atoms; two equivalent Bi atoms and a third Se atom in each quintuple layer (see Fig. 4.1 (c)). There is strong coupling between two atomic layers within one quintuple layer but there exists much weaker couling (van der Waals type) between two quintuple layers. The primitive lattice vectors (t_1, t_2, t_3) are shown in Fig. 4.1 (a). The Se2 site (see Fig. 4.1 (c)) plays the role of inversion centre. We have used 2×2×1 supercell with two quintuple layers containing 40 atoms for the simulation. The vacuum layer in the supercell is considered as 20 Å to avoid the artificial interlayer interactions (see Fig. 4.2). According to the experimental observations, in the presence of water, Bi_2Se_3 surface is modified through some reaction. To study this effect, we consider surface adsorption of water on the Bi_2Se_3 surface. We start with adsorption of one water molecule on the Bi_2Se_3 surface. We test for all the possible sites for the water adsorption. We find that the most preferable binding site is in between two Se atoms rather than on top of the Se atoms on topmost Bi_2Se_3 surface. For the water adsorption in this preferred binding site, we consider two, four and eight water molecules.

The height of water molecule from the Bi_2Se_3 surface is found to be 5.00 Å, 3.91 Å, 3.24 Å and 2.14 Å for one, two, four and eight water molecules respectively (see Fig. 4.3).

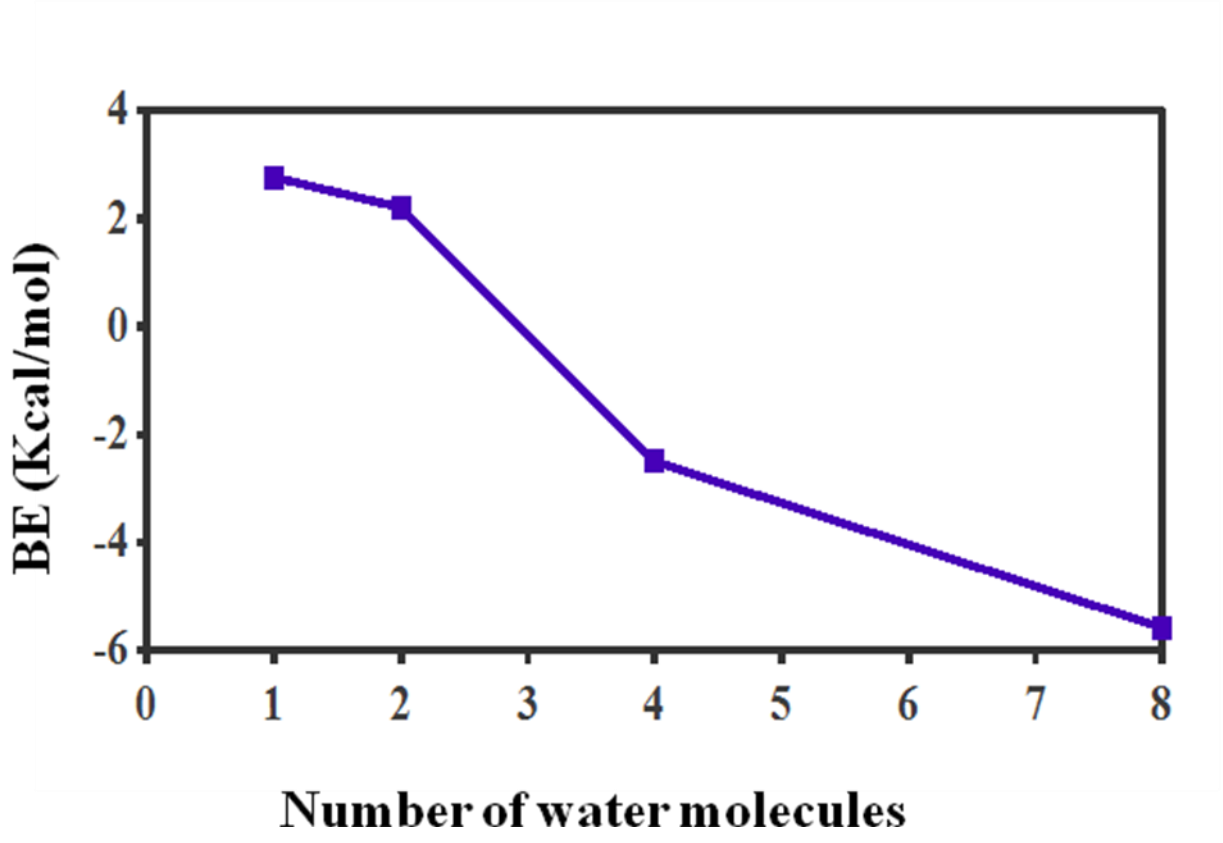

Figure 4.23. Binding energy for different number of water molecules.

This manifests a low sticking coefficient for water which is consistent with experimental observation [23]. Experimentally it was found that after exposure to several hundred Langmuir of water, there is little change in the surface band structure. It is interesting to note that the intermolecular distance between the water molecules is comparable with hydrogen bond distance. So the hydrogen bond is important for the reaction of water with Bi_2Se_3 surface. The binding energies are calculated with the formula given by

$$BE = E_{Bi_2Se_3.nH_2O} - [E_{Bi_2Se_3} + nH_2O]$$

Here BE is the binding energy; $E_{Bi2Se3.nH2o}$ is energy of Bi_2Se_3 and H_2o together, E_{Bi2Se3} is the energy of Bi_2Se_3 and nH_20 is the energy of the n number of water molecules.

Fig. 4.14 shows that our calculated binding energy for various number of water molecule. We see that as the number of water molecules increase, the binding energy becomes more negative, favoring interactions stabilizations. We find that as the amount of water molecules increases, the water adsorption on the Bi_2Se_3 surface becomes more favorable.

4.4 Conclusions

We have presented an introductory study on the surface of topological insulator, Bi_2Se_3. Our study shows that the reaction between surface states of Bi_2Se_3 and water is favorable when the surface is exposed to huge amount of water. This finding is consistent with experimental observations. We find that hydrogen bonding is important for this reaction.

Reference

(1) C. L. Kane and E. J. Mele. Phys. Rev.Lett. 95, 146802 (2005)

(2) J. E. Moore and L. Balents. Phys.Rev.B. 75,121306 (2007)

(3) Liang Fu, C. L. Kane, and E. J. Mele. Phys. Rev. Lett. 98, 106803 (2007)

(4) M. Z. Hasan and C. L. Kane. Rev. Mod. Phys. 82, 3045 (2010)

(5) Haijun Zhang, Chao-Xing Liu, Xiao-Liang Qi, Xi Dai1, Zhong Fang and Shou-Cheng Zhang. Nature Physics 5, 438 (2009)

(6)Y. L. Chen, J. G. Analytis, J.-H. Chu, Z. K. Liu, S.-K. Mo, X. L. Qi, H. J. Zhang, D. H. Lu, X. Dai, Z. Fang, S. C. Zhang, I. R. Fisher, Z. Hussain, Z.-X. Shen. Science.325, 178 (2009)

(7) D. Hsieh1, Y. Xia, D. Qian1, L. Wray, F. Meier, J. H. Dil, J. Osterwalder, L. Patthey, A. V. Fedorov, H. Lin, A. Bansil, D. Grauer, Y. S. Hor, R. J. Cava, and M. Z. Hasan. Phys. Rev. Lett. 103, 146401 (2009)

(8) By Yao-Yi Li, Guang Wang, Xie-Gang Zhu, Min-Hao Liu, Cun Ye, Xi Chen, Ya-Yu Wang, Ke He, Li-Li Wang, Xu-Cun Ma, Hai-Jun Zhang, Xi Dai, Zhong Fang, Xin-Cheng Xie, Ying Liu, Xiao-Liang Qi, Jin-Feng Jia, Shou-Cheng Zhang, and Qi-Kun Xue. Adv.Mater. 22, 4002-4007 (2010)

(9) Binghai Yan, Chao-Xing Liu, Hai-Jun Zhang, Chi-Yung Yam, Xiao-Liang Qi, Thomas Frauenheim, and Shou-Cheng Zhang. EPL, 90, 37002 (2010)

(10) K. Kuroda, M. Ye, A. Kimura, S. V. Eremeev, E. E. Krasovskii, E. V. Chulkov, Y. Ueda, K. Miyamoto, T. Okuda, K. Shimada, H. Namatame, and M. Taniguchi. Phys. Rev. Lett. 105, 146801 (2010)

(11) Jeongwoo Kim, Jinwoong Kim, and Seung-Hoon Jhi. Phys. Rev. B. 82, 201312 (2010)

(12) Su-Yang Xu, L. A. Wray, Y. Xia, R. Shankar, A. Petersen, A. Fedorov, H. Lin, A. Bansil, Y. S. Hor, D. Grauer, R. J. Cava, M. Z. Hasan. arXiv:1007.5111v1

(13) Y. S. Hor1, A. J. Williams1, J. G. Checkelsky, P. Roushan, J. Seo, Q. Xu, H. W. Zandbergen, A. Yazdani, N. P. Ong and R. J. Cava. Phys. Rev. Lett. 104, 057001 (2010)

(14) Y. L. Chen, J.-H. Chu, J. G. Analytis, Z. K. Liu, K. Igarashi, H.-H. Kuo, X. L. Qi, S. K. Mo, R. G. Moore, D. H. Lu, M. Hashimoto, T. Sasagawa, S. C. Zhang, I. R. Fisher, Z. Hussain, Z. X. Shen. Science 325,659 (2010)

(15) Steve M. Young, Sugata Chowdhury, Eric J. Walter, Eugene J. Mele, Charles L. Kane and Andrew M. Rappe. Phys. Rev. B. 84, 085106 (2011)

(16) Tsuneya Ando, Alan B. Fowler and Frank Stern. Rev. Mod. Phys. 54, 437-672 (1982)

(17) W.Monch,semiconductor surfaces and interfaces(springer,new York,1993)

(18) Bychkov Yu. A. , Rashba E. I. JETP Lett. 39, 78 (1984)

(19) Y. S. Hor, A. Richardella, P. Roushan, Y. Xia, J. G. Checkelsky, A. Yazdani, M. Z. Hasan, N. P. Ong, and R. J. Cava. Phys. Rev. B. 79, 195208 (2009)

(20) P. D. C. King, R. C. Hatch, M. Bianchi, R. Ovsyannikov, C. Lupulescu, G. Landolt, B. Slomski, J. H. Dil, D. Guan, J. L. Mi, E. D. L. Rienks, J. Fink, A. Lindblad, S. Svensson, S. Bao, G. Balakrishnan, B. B. Iversen, J. Osterwalder, W. Eberhardt, F. Baumberger, and Ph. Hofmann. Phys. Rev. Lett. 107, 096802 (2011)

(21) Haim Beidenkopf, Pedram Roushan, Jungpil Seo, Lindsay Gorman, Ilya Drozdov,

Yew San Hor, R. J. Cava and Ali Yazdani. Nature Physics 7, 939-943 (2011)

(22) Y. L. Chen, J.-H. Chu, J. G. Analytis, Z. K. Liu, K. Igarashi, H.-H. Kuo, X. L. Qi, S. K. Mo, R. G. Moore, D. H. Lu, M. Hashimoto, T. Sasagawa, S. C. Zhang, I. R. Fisher, Z. Hussain and Z. X. Shen. Science 329, 659-662 (2010)

(23) Hadj M. Benia, Chengtian Lin, Klaus Kern, and Christian R. Ast. Phys. Rev. Lett. 107, 177602 (2011)